T Cell Calcium Dynamics Visualized in a Ratiometric tdTomato-GCaMP6f Transgenic Reporter Mouse

Tobias X. Dong[1,2], Shivashankar Othy[1,2], Amit Jairaman[1], Jonathan Skupsky[1,3], Angel Zavala[1], Ian Parker[1,4], Joseph L. Dynes[1], and Michael D. Cahalan[1,5]

[1]Department of Physiology and Biophysics, University of California, 285 Irvine Hall, Irvine, California 92697, USA.

[2]Co-first authors

[3]Department of Medicine, University of California, 285 Irvine Hall, Irvine, California 92697, USA.

[4]Department of Neurobiology & Behavior, University of California, McGaugh Hall, Irvine, California 92697, USA.

[5]Institute for Immunology, University of California, 285 Irvine Hall, Irvine, California 92697, USA.

*Corresponding Author: Michael D. Cahalan (mcahalan@uci.edu)

Key Words: T cell motility, Orai1, genetically encoded Ca^{2+} indicator, Ca^{2+} signaling, two-photon microscopy

Abstract

Calcium is an essential cellular messenger that regulates numerous functions in living organisms. Here we describe development and characterization of “Salsa6f”, a fusion of GCaMP6f and tdTomato optimized for cell tracking while monitoring cytosolic Ca^{2+}, and a transgenic Ca^{2+} reporter mouse with Salsa6f targeted to the Rosa26 locus for Cre-dependent expression in specific cell types. The development and function of T cells was unaffected in Cd4-Salsa6f mice. We describe Ca^{2+} signals reported by Salsa6f during T cell receptor activation in naïve T cells, helper Th17 T cells and regulatory T cells, and Ca^{2+} signals mediated in T cells by an activator of mechanosensitive Piezo1channels. Transgenic expression of Salsa6f enables ratiometric imaging of Ca^{2+} signals in complex tissue environments found in vivo. Two-photon imaging of migrating T cells in the steady-state lymph node revealed both cell-wide and localized sub-cellular Ca^{2+} transients (“sparkles”) as cells migrate.

Introduction

Calcium (Ca^{2+}) is an essential second messenger responsible for a wide variety of cellular functions (Berridge, Lipp et al. 2000, Clapham 2007, Berridge 2012). Through the use of synthetic small molecule Ca^{2+} indicators such as fura-2 and fluo-4, imaging studies have greatly expanded our understanding of Ca^{2+} signaling dynamics (Tsien, Pozzan et al. 1982, Grynkiewicz, Poenie et al. 1985). However, such indicators cannot be targeted to specific subcellular compartments or cell populations, and are unsuitable for long-term studies due to leakage out of cells. Moreover, they often do not faithfully report pure cytosolic Ca^{2+} signals, because of diffusion into cellular compartments such as the nucleus. One alternative to overcoming these limitations is with genetically encoded Ca^{2+} indicators (GECIs), first developed two decades ago as FRET-based fluorescence probes (Miyawaki, Llopis et al. 1997, Romoser, Hinkle et al. 1997, Perez Koldenkova and Nagai 2013). Key advantages to GECIs include the capability for genetic targeting to specific cell types or subcellular organelles, measuring local Ca^{2+} levels by direct fusion to a protein of interest, modulation of expression levels by inclusion of an inducible promoter, and long term studies due to continuous expression of the genetic indicator (Miyawaki, Llopis et al. 1997, Perez Koldenkova and Nagai 2013). Despite these inherent advantages, the initial FRET-based GECI probes were not widely used as their performance fell far behind small molecule Ca^{2+} indicators, particularly in Ca^{2+} sensitivity, brightness, and dynamic range. Since then, successive rounds of design and contributions from multiple research groups have resulted in numerous variants of GECIs with high dynamic range and dramatically improved performance (Baird, Zacharias et al. 1999, Nakai, Ohkura et al. 2001, Tian, Hires et al.

2009, Zhao, Araki et al. 2011, Akerboom, Chen et al. 2012, Akerboom, Carreras Calderon et al. 2013, Chen, Wardill et al. 2013). Single fluorescent protein-based GECIs containing a circularly permutated green fluorescent protein (GFP) exhibit high brightness, fast response kinetics, and offer multiple color variants, including the GECO and the GCaMP series (Tian, Hires et al. 2009, Zhao, Araki et al. 2011, Akerboom, Chen et al. 2012, Chen, Wardill et al. 2013). FRET-based GECIs have continued to evolve as well, with sequential improvements including incorporation of circularly permuted yellow fluorescent proteins (cpYFPs) to improve dynamic range in the yellow cameleon (YC) family (Nagai, Yamada et al. 2004), use of troponin C as the Ca^{2+} sensing element in the TN indicator family (Heim and Griesbeck 2004), computational redesign of the calmodulin-M13 interface to increase the range of Ca^{2+} sensitivity and reduce perturbation by native calmodulin in the DcpV family (Palmer, Giacomello et al. 2006), and complete redesign of the troponin C domain to increase response kinetics and reduce buffering of cytosolic Ca^{2+} in the TN-XXL family (Mank, Reiff et al. 2006, Mank, Santos et al. 2008).

The latest generation of GECIs have crossed key performance thresholds previously set by small-molecule indicators, enabling GECIs to be widely applied in diverse Ca^{2+} imaging studies without sacrificing performance. Members of the GCaMP6 family are capable of tracking cytosolic Ca^{2+} changes from single neuronal action potentials, with higher sensitivity than small-molecule indicators such as OGB-1 (Chen, Wardill et al. 2013). The availability of multicolored variants in the GECO family and the RCaMP series allowed for simultaneous measurement of Ca^{2+} dynamics in different cell populations in the same preparation, or in different subcellular compartments within the

same cell (Zhao, Araki et al. 2011, Akerboom, Carreras Calderon et al. 2013). These variants can be integrated with optogenetics to simultaneously evoke channel rhodopsin activity while monitoring localized Ca^{2+} responses in independent spectral channels (Akerboom, Carreras Calderon et al. 2013). Moreover, individual GECIs can be tagged onto membrane Ca^{2+} channels to directly measure Ca^{2+} influx through the target channel of interest, enabling optical recording of single channel activity without the need for technique-intensive patch clamping (Dynes, Amcheslavsky et al. 2016).

Another advantage of GECIs is their capability to be incorporated into transgenic organisms. Although several GECI-expressing transgenic mouse lines have already been reported, many of these studies used older variants of GECIs that are expressed only in selected tissues (Hasan, Friedrich et al. 2004, Ji, Feldman et al. 2004, Tallini, Ohkura et al. 2006, Heim, Garaschuk et al. 2007). The Ai38 mouse line overcomes these issues by combining GCaMP3 with a robust and flexible Cre/lox system for selective expression in specific cell populations (Zariwala, Borghuis et al. 2012). Based on a series of Cre-responder lines designed for characterization of the whole mouse brain (Madisen, Zwingman et al. 2010), the Ai38 mouse line contains GCaMP3 targeted to the Rosa26 locus but requires Cre recombinase for expression. By crossing Ai38 with various Cre mouse lines, GCaMP3 can be selectively expressed in specific cell populations. Thus, target cells may be endogenously labeled without invasive procedures, avoiding potential off-target side effects reported in GECI transgenic lines with global expression (Direnberger, Mues et al. 2012). The newly released PC::G5-tdT mouse line provides improved functionality by targeting a Cre-dependent GCaMP5G-IRES-tdTomato transgenic cassette to the *Polr2a* locus (Gee, Smith et al. 2014).

However, in the PC::G5-tdT mouse line, GCaMP5G and tdTomato are expressed individually, and localize to different cell compartments. Moreover, because expression of tdTomato is driven by an internal ribosomal entry site, the expression level is highly variable and weaker than GCaMP5G, limiting identification of positive cells and preventing accurate ratiometric measurements.

Although single fluorescent protein-based indicators have high brightness and fast response kinetics, as non-ratiometric probes they are problematic for Ca^{2+} imaging in motile cells where fluorescence changes resulting from movement may be indistinguishable from actual changes in Ca^{2+} levels. Here, we introduce a novel genetically encoded Ca^{2+} indicator - that we christen 'Salsa6f' - by fusing green GCaMP6f to the Ca^{2+}-insensitive red fluorescent protein tdTomato. This probe enables true ratiometric imaging, in conjunction with the high dynamic range of GCaMP6. We further describe the generation of a transgenic mouse enabling Salsa6f expression in a tissue-specific manner, and demonstrate its utility for imaging T lymphocytes in vitro and in vivo.

Results

A novel ratiometric genetically encoded Ca^{2+} indicator, Salsa6f

In order to develop a better tool to monitor Ca^{2+} signaling in T cells both in vivo and in vitro, we first evaluated the latest generation of genetically encoded Ca^{2+} indicators (GECIs) (Zhao, Araki et al. 2011, Chen, Wardill et al. 2013). We transiently expressed and screened a variety of single fluorescent protein-based GECIs in HEK 293A cells (**Figure 1A**), and selected GCaMP6f based on fluorescence intensity, dynamic range, and Ca^{2+} affinity suitable for detecting a spectrum of cytosolic Ca^{2+} signals (K_d = 375 nM). To enable cell tracking even when basal Ca^{2+} levels evoke little GCaMP6f fluorescence, we fused GCaMP6f to the Ca^{2+}-insensitive red fluorescent protein tdTomato, chosen for its photostability and efficient two-photon excitation (Drobizhev, Makarov et al. 2011). A V5 epitope tag (Lobbestael E 2010) served to link tdTomato to GCaMP6f (**Figure 1B**). The resultant ratiometric fusion indicator, coined "Salsa6f" for the combination of red tdTomato with the green GCaMP6f, was readily expressed by transfection into HEK 293A cells and human T cells. Salsa6f exhibited a ten-fold dynamic range, with a brightness comparable to GCaMP6f alone (**Figure 1A,C**). For two-photon microscopy, both components of Salsa6f can be visualized by femtosecond excitation at 900 nm (**Figure 1D**). GCaMP6f produces increased green fluorescence during elevations in cytosolic Ca^{2+}, while tdTomato provides a stable red fluorescence that facilitates cell tracking and allows for ratiometric Ca^{2+} imaging (**Figure 1D; Video 1**). Salsa6f is excluded from the nucleus, ensuring accurate measurement of cytosolic Ca^{2+} fluctuations (**Figure 1D,E**). When expressed by transfection in human T cells,

Salsa6f reported Ca^{2+} oscillations induced by immobilized αCD3/28 antibodies with a high signal to noise ratio and time resolution (**Figure 1E,F**).

Generation of Salsa6f transgenic reporter mice and validation in immune cells

Guided by the transgenic targeting strategy for the Ai38 mouse line (Zariwala, Borghuis et al. 2012), we inserted Salsa6f into a Gt(ROSA)26Sor5'-pCAG-FRT-LSL-Salsa6f-WPRE-bGHpA-AttB-FRT-NeoR-AttP-Gt(ROSA)26Sor3' cassette, then targeted it to the Rosa26 locus in JM8.N4 mouse embryonic stem (ES) cells (**Figure 2A**). Cells positive for the allele *Gt(ROSA)26Sor*$^{pCAG\text{-}FRT\text{-}LSL\text{-}Salsa6f\text{-}WPRE\text{-}bGHpA\text{-}AttB\text{-}FRT\text{-}NeoR\text{-}AttP}$ were selected by neomycin resistance, and correctly targeted clones were screened by Southern blot (**Figure 2B**), then injected into C57BL/6J blastocysts for implantation. Chimeric pups carrying the Salsa6f transgene were identified by PCR screening for the *Nnt* gene, as the initial JM8.N4 ES cells were *Nnt*$^{+/+}$ while the C57BL/6J blastocysts were *Nnt*$^{-/-}$ (**Figure 2C**). Positive chimeras were bred to R26ΦC31o mice to remove the neomycin resistance gene and to produce LSL-Salsa6f F1 founders that are heterozygotic for the *Gt*(*ROSA*)*26Sor*$^{pCAG\text{-}FRT\text{-}LSL\text{-}Salsa6f\text{-}WPRE\text{-}bGHpA\text{-}AttB/P}$ allele, then further bred to generate homozygotic mice which we term LSL-Salsa6f (Hom).

LSL-Salsa6f (Hom) mice were bred to *Cd4*$^{Cre+/+}$ mice to obtain reporter mice heterozygous for Salsa6f, designated as Cd4-Salsa6f (Het) mice from here on, that selectively express Salsa6f in T cells (**Figure 3A**). Mice homozygous for Salsa6f are designated as Cd4-Salsa6f (Hom). Salsa6f was detected by tdTomato fluorescence on flow cytometry. 88% of these Salsa6f^{+} cells in thymus were double positive for Cd4 and Cd8 (**Figure 3B**). This is due to the double-positive stage during development, in which developing thymocytes will express both Cd4 and Cd8 before undergoing positive and

negative selection to become either mature $Cd4^+$ or $Cd8^+$ T cells. Salsa6f was readily detected by the red tdTomato signal in cells from spleen (40%), lymph node (57%), and thymus (93%) (**Figure 3C**). As expected, double positive cells were not detected in the spleen (**Figure 3D**). More than 98% of $Cd4^+$ and $Cd8^+$ T cells from these reporter mice were positive for Salsa6f. Salsa6f was also detected in 5% of $Cd19^+$ cells and 3% of $Cd11b^+$ cells (**Figure 3E**). A small fraction of B cells express Cd4 mRNA, which may explain the presence of Salsa6f in $Cd19^+$ cells (Zhang and Henderson 1994). $Cd11b^+$ cells positive for Salsa6f may be splenic resident dendritic cells that also express Cd4 (Vremec, Pooley et al. 2000, Turley, Fletcher et al. 2010). The total number and relative frequencies of $Cd4^+$, $Cd8^+$, $Cd19^+$, and $Cd11b^+$ cells were similar to the *Cd4*^{Cre} controls (**Figure 3F,G**).

To determine whether expression of Salsa6f might affect functional responses downstream of Ca^{2+} signaling in T cells, we first purified $Cd4^+$ T cells and monitored cell proliferation in vitro during TCR engagement of αCd3 and co-stimulating αCd28 antibodies attached to activating beads. Both hetero and homozygotic Salsa6f-expressing $Cd4^+$ T cells proliferated similar to the *Cd4*^{Cre} controls (**Figure 4A,B**). To further probe functional responses, we differentiated naive $Cd4^+$ T cells using polarizing cytokine stimuli to generate Th1, Th17 and induced regulatory T cells (iTregs). Salsa6f positive naïve $Cd4^+$ T cells from both Cd4-Salsa6f (Het) and Cd4-Salsa6f (Hom) mice readily differentiated into various helper T cell subtypes similar to the *Cd4*^{Cre} controls (**Figure 4C-E and Figure 4-figure supplement 1**). In addition, as described in the companion paper, adoptively transferred Salsa6f positive cells readily homed to lymph nodes and exhibited normal motility characteristics (Dong, Othy et al. 2017). In

summary, our results demonstrate normal T cell functions of Salsa6f-expressing T lymphocytes with respect to development, cellular phenotype, cell proliferation, differentiation, homing, and motility.

Single-cell ratiometric Ca^{2+} measurement in Cd4-Salsa6f reporter mice

$Cd4^+$ T cells were purified from Cd4-Salsa6f (Het) reporter mice, stimulated with plate-bound αCd3/28 antibodies for two days, and imaged by confocal microscopy while still in contact with immobilized antibodies (**Figure 5A, Video 2**). Activated $Cd4^+$ T cells expressing Salsa6f exhibited stable red fluorescence and wide fluctuations in green fluorescence due to Ca^{2+} oscillations resulting from T cell receptor engagement (**Figure 5B**). Despite variability in total fluorescence between cells due to individual differences in cell size, the basal and peak green/red Salsa6f ratios (referred from now on as G/R ratio for GCaMP6f/tdTomato intensity) were comparable between cells and showed up to six-fold increases during peaks in Ca^{2+} fluctuations (**Figure 5C**). Flow cytometric analysis of Salsa6f mouse T cells revealed a thirteen-fold increase in G/R ratio, by pretreatment with ionomycin in Ca^{2+}-free medium to deplete cytosolic Ca^{2+} followed by addback of extracellular Ca^{2+}, further emphasizing the high dynamic range of Salsa6f (**Figure 5D**). Finally, to test if increasing the genetic dosage can improve the brightness of Salsa6f, we compared $Cd4^+$ T cells from Cd4-Salsa6f (Het) and Cd4-Salsa6f (Hom) mice. T cells from homozygous mice with two allelic copies of the Salsa6f reporter cassette exhibited almost a two-fold increase in tdTomato fluorescence compared to heterozygous mice (**Figure 5E**), allowing for genetic control of Salsa6f expression level when brightness is an issue.

Cytosolic localization and calibration of Salsa6f in transgenic T lymphocytes

We first examined the localization of Salsa6f in naïve $Cd4^+$ T cells isolated from Cd4-Salsa6f (Het) mice and in $Cd4^+$ T cells activated for 2 days on plate-bound αCd3/28. Line scans of the confocal images of cells plated on poly-L-lysine-coated coverslips showed that Salsa6f is primarily localized to the cytoplasm and is excluded from the nucleus (**Figure 6A,B**). Increasing the cytosolic Ca^{2+} levels using thapsigargin (TG) in 2 mM Ca^{2+} Ringer's solution caused a selective increase in the GCaMP6f signal, without altering the localization of Salsa6f probe. In contrast, the small-molecule dye Ca^{2+} indicators fluo-4 or fura-2 loaded into $Cd4^+$ T cells from *Cd4*^{Cre} mice are distributed throughout the cell, including the nucleus (**Figure 6C** and data not shown). A different transgenic mouse, PC::G5-tdT utilizes an internal ribosomal entry site to express both tdTomato and GCaMP5G as separate proteins that localize differently (Gee, Smith et al. 2014), with tdTomato distributed throughout the cell including the nucleus and GCaMP5G predominantly in the cytosol (**Figure 6-figure supplement 1**). In contrast, our tandem probe, Salsa6f, results in both red and green fluorescent proteins co-localized in the cytosol, allowing true ratiometric Ca^{2+} imaging and facilitating tracking of cells.

Overlap of GCaMP6f emission and tdTomato excitation spectra raises the possibility of FRET (Forster resonance energy transfer) which would decrease G/R ratio and reduce dynamic range. If there were significant FRET, we would expect acceptor (tdTomato) signal to increase with increase in donor (GCaMP6f) intensity, as shown for GECI probes utilizing GCaMP and mCherry dependent on the rigidity of the linker used (Cho, Swanson et al. 2017). We treated Salsa6f positive T cells with Ringer's buffer containing Ionomycin and different concentrations of Ca^{2+} and measured the steady-

state GCaMP6f and tdTomato fluorescence signals. The GCaMP6f signal increased as expected with increasing Ca^{2+} concentrations, but the tdTomato signal remained unchanged (**Figure 6D**). This suggests that the V5 epitope tag is effective in reducing FRET between GCaMP6f and tdTomato which otherwise may compromise probe performance.

We next characterized the in situ Ca^{2+} affinity of Salsa6f in $Cd4^+$ T cells isolated from Cd4-Salsa6f (Het) mice, using fura-2 as a calibration standard. Fura-2 has an in situ K_d ~ 225 nM at 25º C (Lewis and Cahalan 1989), which is somewhat lower than in vitro K_d values reported for GCaMP6f (Chen, Wardill et al. 2013, Badura, Sun et al. 2014). We used time-lapse imaging to record G/R ratio in response to ionomycin applied with stepwise increases in the external Ca^{2+} concentration and, using identical protocols, compared it to fura-2 Ca^{2+} signals in control $Cd4^+$ T cells from *Cd4*^{Cre} mice (**Figure 6E,F**). To facilitate comparison, fura-2 and Salsa6f ratios were normalized with R_{min}=0 and R_{max}=1. Salsa6f responded with faster rise and decay kinetics than fura-2 to progressive increases in cytosolic Ca^{2+} levels, especially at lower external Ca^{2+} concentrations. Salsa6f responses also saturated at lower cytosolic Ca^{2+} levels than fura-2 responses. This is not altogether surprising given that genetically encoded Ca^{2+} indicators have been reported to have a steeper Hill coefficient than chemical indicators (Badura, Sun et al. 2014). Assuming that Cd4-Salsa6f T cells reach similar Ca^{2+} levels as control *Cd4*^{Cre} cells, we plotted peak and the steady state G/R ratios against the cytosolic Ca^{2+} concentrations obtained from the fura-2 experiment which yielded an estimated in situ K_d for Salsa6f in the range of 160 – 300 nM (**Figure 6G**). Based on

these results, we conclude that Salsa6f is sensitive in detecting cytosolic Ca^{2+} from 100 nM - 2 μM, which is in the range of physiological cytosolic Ca^{2+} signals.

T cell Ca^{2+} signaling in response to Ca^{2+} store depletion, T cell receptor engagement, and mechanical stimulation

TCR engagement activates a canonical Ca^{2+} signaling pathway in T cells, characterized by IP_3-induced Ca^{2+} release from the endoplasmic reticulum, leading to store-operated Ca^{2+} entry (SOCE) through Orai1 channels (Cahalan and Chandy 2009, Prakriya and Lewis 2015). Past studies on T cell Ca^{2+} signaling have largely relied on indicators like fura-2 and fluo-4 which have the potential drawback of being distributed into the nucleus, thus confounding the measurement of pure cytoplasmic Ca^{2+} signals, a problem particularly notable in T cells with their large nuclear to cytoplasmic volume ratio. Salsa6f, with its high dynamic range, ratiometric readout and targeted localization in the cytosol, is thus well suited to record physiological cytosolic Ca^{2+} signals. To this end, we recorded Ca^{2+} signals from 2 day-activated $Cd4^+$ T cells from Cd4-Salsa6f (Het) mice in response to a variety of stimuli.

To study SOCE more directly, we depleted ER Ca^{2+} stores in activated and in naïve T cells by applying TG in Ca^{2+}-free solution. We observed a small but sharp initial peak indicating ER store release followed by a sustained Ca^{2+} signal upon restoring Ca^{2+} to the external bath, indicative of SOCE (**Figure 7A, Video 3 and Figure 7-Figure supplement 1A**). Almost all cells responded to this supra-physiological stimulus (**Figure 7A**, right panel). In contrast, T cells plated on αCd3/28 to activate TCR-induced signaling showed heterogeneous responses, with some exhibiting asynchronous Ca^{2+} oscillations of varying frequencies and durations whereas others failed to respond

(**Figure 7B, Video 4**). Past studies have attributed these Ca^{2+} oscillations to SOCE from repetitive opening and closing of Orai1 channels allowing Ca^{2+} to enter T cells in a periodic and asynchronous manner (Lewis and Cahalan 1989, Dolmetsch and Lewis 1994), unlike the sustained activation with TG treatment. Cells plated on αCd3 alone also showed rhythmic oscillatory Ca^{2+} signals; however, the percentage of responding cells was significantly lower than with αCd3/28, resulting in a lower average signal compared with αCd3/28 stimulation (**Figure 7C, Video 5**) These results suggest that co-stimulatory signaling through Cd28 enhances the response to TCR activated Ca^{2+} signals, in alignment with previous observations (Chen and Flies 2013).

Finally, we focused on a novel Ca^{2+} signaling pathway involving mechanosensitive Ca^{2+}-permeable channels. We examined activation of mechanosensitive channels in Salsa6f^{+} T cells that were plated on αCd3/28-coated glass coverslips, by flowing external solution rapidly past the cells. Perfusion produced a transient rise in the cytosolic Ca^{2+} signal, likely a result of flow shear stress (**Figure 7D and Figure 7-figure supplement 1B**). The Piezo family of mechanosensitive channels plays a vital role in cell motility and development (Nourse and Pathak 2017), but it is not known whether these channels are expressed and play a role in immune cell function. Perfusion of medium including Yoda1, a selective small molecule activator of Piezo1 (Syeda, Xu et al. 2015), resulted in robust Ca^{2+} signals in activated and naïve T cells that were larger and more and sustained than those activated by perfusion of solvent or media alone (**Figure 7D and Figure 7-figure supplement 1C**). In summary, we show Ca^{2+} signals in T cells in response to an activator of Piezo1 channels. These results illustrate the utility of Salsa6f for screening agents that modulate Ca^{2+} signaling

in T cells and open the possibility for further exploration of the functional role of Piezo1 channels in T cell function.

TCR-induced Ca^{2+} signaling in helper T cell subsets

We also monitored Ca^{2+} signaling in response to TCR activation by αCd3/28 in various subsets of T cells from Cd4-Salsa6f (Het) mice, including naïve T cells, Th17 cells and iTregs (**Figure 8A-C**). All subtypes of T cells responded to plate-bound stimulation of αCd3/28 with oscillatory changes in their cytosolic Ca^{2+} levels, very similar to the Ca^{2+} responses in 2 day-activated T cells illustrated in Fig 7B. The responses were heterogeneous, with some cells showing multiple peaks of varying durations and amplitudes, occasional sustained signals and other cells failing to respond. Whereas the overall average responses were not very different between the three subtypes examined, some individual Th17 cells and iTregs showed higher amplitude signals than any naïve T cells, but with a greater percentage of non-responding cells. The Cd4-Salsa6f mouse thus opens up new avenues to study the fundamental nature of Ca^{2+} signals in T cell subsets generated in response to variety of stimuli, and to explore the relationship between patterns of Ca^{2+} signals and specific downstream functions.

Two-photon microscopy of Cd4-Salsa6f T cells in the lymph node.

Using 2-photon microscopy to image lymph nodes from Cd4-Salsa6f (Hom) mice under steady-state conditions we observed sporadic localized elevations of green fluorescence indicative of intracellular Ca^{2+} signaling (**Figure 9A,B**). Imaging conditions were optimized for single-wavelength excitation of both TdTomato and GCaMP6f components of Salsa6f (**Figure 9-figure supplement 1**). Some of the green Salsa6f signals were T cell-sized, and the pattern of red Salsa6f fluorescence observed is

consistent with the exclusion of the Salsa6f indicator from the nucleus **(Figure 9C)**. In addition, we observed numerous bright, transient green fluorescent signals which were much smaller in area (about 2 μm^2 in area) (**Figure 9B,D; Video 6**). We term these fluorescent transients "sparkles", because during rapid playback of time-lapse image streams cells appear to sparkle.

Because T cells move rapidly and are not uniformly distributed in lymph nodes, we developed an image processing approach in order to minimize fluctuations in background fluorescence in order to sensitively identify cell-wide Ca^{2+} signals and sparkles (**Figure 9-figure supplement 2**). Based on the one-to-one correspondence of tdTomato and GCaMP6f, we estimated and subtracted out fluctuations in green fluorescence due to cell movement and distribution. After processing, sparkles were found to occur widely across the imaging field (**Figure 9E-G**), and many reached a characteristic maximum intensity (compare **Figure 9F** and **9G**). The brightness of sparkles and the uniformity of background fluorescence allowed us to use a stringent threshold of signals exceeding 5.4 SD of the background noise level to systematically identify bright sparkles. Hundreds of events with a mean amplitude of 6.5 SD above background were observed in each 25-minute imaging session (one image stack every five seconds), whereas fewer than one event exceeding our threshold was expected to occur from random noise fluctuations. Sparkles were more frequent than cell-wide transients (**Figure 9H**), extended over a median area of 1.9 μm^2 (n=441 sparkles from 3 lymph nodes; **Figure 9I**), and usually lasted for only one or two consecutive frames (**Figure 9J**). Sparkle trace shape differs from that expected for autofluorescent cell processes drifting into the imaging field (**Figure 9K**). Taken together, these

346 observations suggest that sparkles correspond to local Ca^{2+} signals restricted to small
347 subcellular domains of T cells migrating through the lymph node.

348 The high density of expressing fluorescent T cells in the lymph nodes of Cd4-
349 Salsa6f (Hom) mice makes it difficult to visualize and study subcellular Ca^{2+} signals
350 within individual cells. We thus adoptively transferred Cd4-Salsa6f T cells into wild type
351 recipients so these cells could be viewed in isolation at low density. Small green
352 fluorescence transients seen in lymph nodes after adoptive transfer were similar in
353 intensity to transients seen in Cd4-Salsa6f (Hom) lymph nodes (**Figure 10A**). When
354 small, bright, and brief green fluorescence signals were traced back, they were found to
355 originate in red fluorescent Cd4-Salsa6f (Hom) T cells (**Figure 10B-M**). Cell movement
356 was used to define the front and back of labeled T cells for mapping the subcellular
357 location of Ca^{2+} signals. Some sparkles, identified in processed green channel images,
358 were found to selectively localize to the front or back of motile T cells in which both the
359 cell front and back were clearly seen (**Figure 10D,E,J,K**). Green-red channel ratiometric
360 images, enabled by Salsa6f labeling, confirmed differences in Ca^{2+} concentration
361 between front and back, although regions of elevated Ca^{2+} were also observed flanking
362 the nucleus (**Figure 10F,L**). Differences in green-red channel ratiometric pixel
363 intensities between front and back were highly significant (**Figure 10G,M**; $p<0.0001$,
364 Mann Whitney test). Thus, motile T cells exhibit Ca^{2+} signals that are largely restricted
365 to subregions of the cytoplasm, and these Ca^{2+} signals – sparkles – were identified with
366 high signal-to-noise ratio by Salsa6f expression. In a companion paper (Dong, Othy et
367 al. 2017), we use Salsa6f transgenic mice to consider the relationship between Ca^{2+}
368 signals, both cell-wide and local, and T cell motility in the lymph node.

369

Discussion

We introduce Salsa6f, a novel, ratiometric genetically-encoded Ca^{2+} probe. Salsa6f is a fusion of the high performing green fluorescent GECI GCaMP6f and the bright red fluorescent tdTomato. This simple modification imparts powerful capabilities, which facilitate tracking cells in the absence of Ca^{2+} signaling, enable ratiometric imaging to eliminate motility artifacts, and permit convenient single-wavelength femtosecond excitation for two-photon microscopy. Salsa6f addresses a key weakness of single fluorescent protein-based GECIs by enabling tracking of motile cells and identification of cell morphology, even at basal Ca^{2+} levels when GCaMP6f fluorescence is very weak. We generated a transgenic reporter mouse with Cre-dependent expression of Salsa6f, enabling Ca^{2+} signals to be imaged in specific, genetically defined cell types. Transgenic expression of Salsa6f brings the power of ratiometric chemical Ca^{2+} indicators to imaging cellular Ca^{2+} signals amid the complex tissue environments found in vivo.

Salsa6f preserves the exceptional performance of GCaMP6f, which in the presence of high levels of Ca^{2+} is as bright as the standard high performing green fluorescent protein, EGFP (Chen, Wardill et al. 2013). We find that Salsa6f possesses a dynamic range similar to GCaMP6f, and both are superior to FRET-based GECIs (Heim, Garaschuk et al. 2007, Thestrup, Litzlbauer et al. 2014). The Ca^{2+} affinity of Salsa6f, 160-300 nM, is well suited to detecting a variety of cellular Ca^{2+} signals. Inclusion of tdTomato in Salsa6f enables ratiometric imaging, calibration, and measurement of Ca^{2+} concentrations within cells. Moreover, Salsa6f is distributed uniformly throughout the cytosol; its exclusion from the nucleus provides reliable and

393 selective reporting of cytosolic Ca^{2+} signaling. This is in contrast to the recently
394 developed PC::G5-tdT mouse strain in which the tdTomato is found throughout the cell
395 but the separately expressed GCaMP5G is excluded from the nucleus (Gee, Smith et
396 al. 2014).

397 We created a transgenic mouse strain in which Salsa6f is expressed under
398 genetic control using the Rosa26^{Cre} recombinase system, and we used this system to
399 label immune cells that express Cd4. Salsa6f labeling enables readout of cytosolic Ca^{2+}
400 dynamics in T cells in vitro with high dynamic range, without the handling and potential
401 toxicity associated with loading of chemical Ca^{2+} indicators. Indeed, a concern with any
402 Ca^{2+} indicator is whether it may perturb cell function by buffering free Ca^{2+} ions or other
403 means. In $Cd4^{+}$ immune cells, we found no effects of Salsa6f expression, even in Cd4-
404 Salsa6f (Hom) mice, with respect to cellular phenotype, cell proliferation, differentiation,
405 and, in our companion paper (Dong, Othy et al. 2017), homing and T cell motility.

406 Salsa6f was used to detect Ca^{2+} influx due to direct activation of SOCE, TCR
407 stimulation, and an activator of Piezo1 channels – the latter observed in T cells for the
408 first time to our knowledge. We also detected differences in patterns of Ca^{2+} signaling
409 between naïve T cells, Th17 cells, and iTregs. These experiments demonstrate the
410 sensitivity, brightness, uniformity of labeling, and ease of detecting dynamic Ca^{2+}
411 signals using Salsa6f.

412 A primary advance of this work is to take the in vitro capabilities of an excellent
413 Ca^{2+} indicator and bring these into the realm of in vivo imaging. Within tissues, nearby
414 cells exhibit differences, ranging from subtle to dramatic, in morphology, connectivity,
415 and molecular profile. The red fluorescence of Salsa6f, combined with genetic Salsa6f

labeling, associates these characteristics with readout of cellular Ca^{2+} signaling. Both the tdTomato and GCaMP6f in Salsa6f are excited well by a 920 nm femtosecond pulsed wavelength for 2-photon imaging, enabling visualization hundreds of micrometers deep into lymph nodes. The immune system poses additional challenges for imaging because the constituent cells are highly motile. Indeed, direct cell-to-cell interactions of motile immune cells form the basis of immune surveillance (Mrass, Petravic et al. 2010, Krummel, Bartumeus et al. 2016). We were able to readily identify red fluorescent Salsa6f T cells easily in intact lymph nodes following adoptive transfer. Our images reveal uniform red fluorescence labeling by Salsa6f with clear subcellular morphology in imaging sessions encompassing hundreds of time lapse images. Moreover, Salsa6f offers the opportunity not only to record fluctuations in relative Ca^{2+} levels over time, but also to read out absolute Ca^{2+} concentrations within cells. We have measured the affinity of Salsa6f in intact cells; in principle, use of this approach will allow other microscope systems to be calibrated for measuring absolute Ca^{2+} concentrations with Salsa6f. Knowledge of absolute Ca^{2+} concentrations is necessary to develop quantitative models of Ca^{2+} signaling and cell behavior. Indeed, we demonstrate that clear Salsa6f ratio images can be generated from motile T cells in intact lymph nodes.

Our Salsa6f transgenic mouse line enables more sophisticated experimental approaches. One is the ability to detect rare Ca^{2+} signaling events. The high brightness and dynamic range of modern GECIs like Salsa6f contribute to detection of rare Ca^{2+} signaling events inside intact tissues or even whole transgenic animals (Kubo, Hablitzel et al. 2014, Portugues, Feierstein et al. 2014). Ca^{2+} signals have been previously

recorded within lymph nodes in adoptively transferred T cells transgenically expressing doxycycline inducible mCameleon (Le Borgne, Raju et al. 2016), GCaMP3 and dsRed as separate proteins (Shulman, Gitlin et al. 2014), and virally transduced YC-nano-50^{CD} (Liu, Xu et al. 2015). Potential disadvantages of these probes include low dynamic range, nuclear expression of mCameleon and dsRed, the high Ca^{2+} affinity of YC-nano-50^{CD} (50 nM), and lack of ratiometric measurement. Imaging T cells transgenically expressing Salsa6f helps to overcome many of these limitations. Detecting rare events is made harder by inhomogeneities in cell populations of the lymph node as well as the movement of immune cells therein. Because of the one-to-one correspondence of tdTomato and GCaMP6f in Salsa6f, we were able to estimate and subtract resting GCaMP6f fluorescence even in motile cells. This approach substantially improves the uniformity of the fluorescence background upon which rare Ca^{2+} signaling events can be detected. Reliable and uniform cytosolic labeling contributes as well. Combined, these factors enabled us to detect not only sporadic cell-wide Ca^{2+} elevations, but also sparkles, much smaller sporadic local Ca^{2+} signals. The sensitivity and resolution of these images are sufficient to map local signals from intact lymph nodes to sub-regions of T cells. Moreover, while we focused upon the brightest local Ca^{2+} signals to demonstrate their existence, we expect that Salsa6f will enable even lower intensity Ca^{2+} signals to be linked to subcellular mechanisms and, ultimately, resulting cell behaviors. In a companion paper (Dong, Othy et al. 2017) we capitalize on the unique properties of Salsa6F to relate Ca^{2+} signals, both global and local, to T cell motility in the intact lymph node.

462 **Acknowledgments**

463 We acknowledge the UC Irvine Transgenic Mouse Facility for support in making the
464 transgenic mouse, Dr. Grant MacGregor from the UC Irvine Department of
465 Developmental and Cell Biology for excellent advice, and Dr. Jennifer Atwood of the
466 Flow Core Facility supported by the UC Irvine Institute of Immunology. We also thank
467 Andy Yeromin for advice on curve-fitting. This work was supported by an R21 grant
468 AI117555, and RO1 grants NS14609 and AI121945, from the National Institutes of
469 Health (MDC), and by a postdoctoral fellowship from the George E. Hewitt Foundation
470 for Medical Research (A.J.).

471

Methods

Key Resources table

Reagent type (species) or resource	Designation	Source or reference	Identifiers	Additional information
Recombinant DNA reagent	Salsa6f	this paper		Fusion of GCaMP6f to tdTomato via a V5 epitope linker (GCaMP6f-V5-tdTomato)
Recombinant DNA reagent	Gt(ROSA)26Sor5'-pCAG-FRT-LSL-Salsa6f-WPRE-bGHpA-AttB-FRT-NeoR-AttP-Gt(ROSA)26Sor3' cassette	this paper		Salsa6f inserted into a Gt(ROSA)26Sor-pCAG-LSL-(Salsa6f)-WPRE-bGHpA-NeoR cassette.
Transgene (mouse)	*Gt(ROSA)26Sor^{pCAG}-FRT-LSL-Salsa6f-WPRE-bGHpA-AttB-FRT-NeoR-AttP*	this paper		Allele with the above cassette targeted to the ROSA26 locus.
Transgene (mouse)	*Gt(ROSA)26Sor^{pCAG}-FRT-LSL-Salsa6f-WPRE-bGHpA-AttB/P*	this paper		Same as above with Neomycin cassette deleted

strain, strain background (mouse)	LSL-Salsa6f (F1), LSL-Sals6f (Hom)	this paper		Salsa6f transgene targeted to Rosa26 locus in JM8.N4 mouse embryonic stem (ES) cells. Positive chimeras bred to R26ΦC31o mice to produce LSL-Salsa6f F1 founders and homozygotic LSL-Salsa6f (Hom) mice. See Materials and methods for details.
strain, strain background (mouse)	Cd4-Salsa6f (Het), Cd4-Salsa6f (Hom)	this paper		LSL-Salsa6f (Hom) mice crossed to *Cd4*^{Cre} mice to produce heterozygotic and homozygotic *Salsa6f-Cd4*^{Cre} mice (designated as Cd4-*Salsa6f*$^{+/-}$

				and *Cd4-Salsa6f*$^{+/+}$ in the paper).
strain, strain background (mouse)	*Cd4*^{Cre} *mice C57BL/6J*	Jackson #017336		
strain, strain background (mouse)	C57BL/6J	Jackson #000664		
cell line (human)	HEK293A	Invitrogen (#R705-07)		
transfected construct (synthetic)	Salsa6f	this paper		see above for *Salsa6f* gene
transfected construct (synthetic)	G-GECO1, B-GECO1, GCaMP6f, GCaMP6m, GCaMP6s	Addgene		
antibody	anti-mouse IL-4, IL17A-APC (clone TC11-18H10.1), IFN-Pacific Blue (clone XMG1.2)	BioLegend		
antibody	Foxp3-PE (clone FJK16s)	ThermoFisher Scientific		
antibody	αCd3 and αCd28	Invivogen		
antibody	αCd3 and αCd28	LifeTechnologies		

	coated dynabeads	Corp.		
peptide, recombinant protein	recombinant human TGFβ1	Tonbo Biosciences		
peptide, recombinant protein	recombinant mouse IL-12, IL-23, IL-1β, TGFβ	BioLegend		
peptide, recombinant protein	recombinant human IL-2	BioLegend		
commercial assay or kit	EasySep mouse naïve Cd4 T cell isolation kit	Stem Cell Technologies		
commercial assay or kit	EasySep mouse Cd4 T cell isolation kit	Stem Cell Technologies		
chemical compound, drug	Cell trace violet, eFluor® 780	ThermoFisher Scientific		
chemical compound, drug	Ionomycin, Thapsigargin, Retinoic Acid, PMA	Sigma Aldrich		
chemical compound, drug	Ghost dye 780	Biolegend		
chemical compound, drug	Fura2-AM, Fluo-4 AM	ThermoFisher Scientific		
software, algorithm	ImageJ/ Fiji	NIH		
software, algorithm	IMARIS	Bitplane		
other	35mm glass chamber	LabTek, ThermoFisher		

		Scientific		
other	RPMI cell culture medium	Lonza		

GECI screening and Salsa6f plasmid generation

Plasmids encoding GECIs (GECO and GCaMP6) were obtained from Addgene for screening in live cells. HEK 293A cells (Invitrogen- Life Technologies # R705-07) were screened for viruses and mycoplasma, split and frozen into working stocks, cultured using aseptic techniques, and used to evaluate candidate genetically encoded Ca^{2+} indicators. Each probe was cotransfected with Orai1 and STIM1 into HEK 293A cells using Lipofectamine 2000 (Invitrogen, Carlsbad, CA) for 48 hr before screening on an epifluorescence microscope. For construction of Salsa6f, a plasmid for tdTomato (Addgene, Cambridge, MA) and the pEGP-N1 vector (Clontech, Mountain View, CA) was used as a backbone. GCaMP6f was amplified via PCR with N- and C-terminal primers (5' CACAACCGGTCGCCACCATGGTCGACTCATCACGTC 3' and 5' AGTCGCGGCCGCTTTAAAGCTTCGCTGTCATCATTTGTAC 3') and ligated into pEGFP-N1 at the AgeI/NotI sites to replace the eGFP gene, while tdTomato was amplified via PCR with N- and C-terminal primers (5' ATCCGCTAGCGCTACCGGTCGCC 3' and 5' TAACGAGATCTGCTTGTACAGCTCGTCCATGCC 3') and ligated into the backbone at the NheI/BglII sites. An oligo containing the V5 epitope tag was synthesized with sense and antisense strands (5' GATCTCGGGTAAGCCTATCCCTAACCCTCTCCTCGGTCTCGATTCTACG 3' and 5' GATCCGTAGAATCGAGACCGAGGAGAGGGTTAGGGATAGGCTTACCCGA 3') and

ligated into the backbone at the BglII/BamHI sites, linking tdTomato to GCaMP6f and creating Salsa6f. The amplified regions of the construct were verified by sequencing (Eton Bioscience Inc., San Diego, CA). This plasmid, driven by the CMV promoter, was used for transient transfections in HEK 293A cells with Lipofectamine 2000 and in primary human T cells with Amaxa Nucleofection.

Transgenic mouse generation and breeding

The transgenic cassette in **Figure 2B** was generated by inserting Salsa6f, from the plasmid described above, into the Ai38 vector (Addgene Plasmid #34883) and replacing GCaMP3. The final targeting vector included the CAG (cytomegalovirus early enhancer/chicken β-actin) promoter, an LSL sequence with LoxP-STOP-LoxP, the Salsa6f probe (tdTomato-V5-GCaMP6f), the woodchuck hepatitis virus posttranscriptional regulatory element (WPRE), and a neomycin resistance gene (NeoR), all flanked by 5' and 3' Rosa26 homology arms of 1.1 and 4.3 kb. The targeting vector was linearized with PvuI and electroporated into JM8.N4 mouse embryonic stem (ES) cells of C57BL/6N background. Following selection with G418, clones carrying the *Gt(ROSA)26Sor*$^{pCAG\text{-}FRT\text{-}LSL\text{-}Salsa6f\text{-}WPRE\text{-}bGHpA\text{-}AttB\text{-}FRT\text{-}NeoR\text{-}AttP}$ allele were screened by Southern blotting after digestion with HindIII for the 5' end or BglI for the 3' end. Four correctly targeted clones were expanded and checked by chromosome counting, then two clones with >90% euploidy were further expanded and injected into C57BL/6J blastocysts for implantation into pseudopregnant foster mothers. Presence of the Salsa6f transgenic cassette was detected in the resulting chimeric pups by PCR screening for the *Nnt* gene, as the initial JM8.N4 ES cells are *Nnt*$^{+/+}$ while the C57BL/6J blastocysts are *Nnt*$^{-/-}$. Finally, positive chimeras were bred to R26ΦC31o mice (JAX

#007743) to remove the neomycin resistance gene flanked by AttB and AttP sites in the original transgenic cassette, and to produce F1 founders carrying the allele *Gt(ROSA)26Sor*$^{pCAG\text{-}FRT\text{-}LSL\text{-}Salsa6f\text{-}WPRE\text{-}bGHpA\text{-}AttB/P}$ at the Rosa26 locus. These F1 founders were then bred to homozygosity to generate LSL-Salsa6f (Hom) mice, and subsequently crossed to homozygotic *Cd4*^{Cre} mice (JAX #017336) to generate Cd4-Salsa6f (Het) mice expressing Salsa6f only in T cells. *Cd4-Salsa6f* mice were further bred to generate homozygotic Cd4-Salsa6f (Hom) mice for increased Salsa6f expression and fluorescence.

T cell proliferation and differentiation

For T cell proliferation: Cd4 T cells were isolated from spleen and lymph nodes of 6-10 week old mice using negative selection (StemCell Technologies, Cambridge, MA). CellTrace Violet (CTV)-labeled T cells were co-cultured with αCd3/Cd28 coated dynabeads (Life Technologies Corp., Grand Island, NY) at 1:1 ratio according to the manufacturer's protocol in a U bottom 96 well plate. *For T cell differentiation*: Naïve Cd4 T cells were differentiated on activating polystyrene surface (Corning Inc., Corning, NY) with plate-bound αCd3 (2.5 µg/ml) and αCd28 (2.5 µg/ml) in the presence of cytokines for 6 days (Yosef, Shalek et al. 2013)**.** For Th1 differentiation: 25 ng/mL rmIL-12 (BioLegend, San Diego, CA), 10 µg/mL αmouse IL4 (Biolegend). For Th17 differentiation: 2.5 ng/mL rhTGF-β1 (Tonbo Biosciences, San Diego, CA), 50 ng/mL rmIL-6 (Tonbo Biosciences), 25 ng/ml rmIL-23 (BioLegend), and 25 ng/ml rmIL-β1 (BioLegend). For iTreg differentiation: 10 ng/mL rhTGF-β1, 100 units/mL of rmIL-2 (BioLegend), 5 µM Retinoic Acid (Sigma, St. Louis, MO).

Flow cytometry.

CTV dilution assay was performed in live cells (Fixable Viability Dye eFluor® 780 negative gating; Thermofisher Scientific Inc., Grand Island, NY). To detect intracellular cytokines, 6 day differentiated cells were stimulated in with 25 ng of phorbol 12-myristate 13-acetate (PMA), 1 μg ionomycin (Sigma), and monensin (Golgistop® BD biosciences) for 4 hr at 37 ℃. Dead cells were labeled with Ghost dye 780 (BioLegend), then washed, fixed, permeabilized using FoxP3 staining buffer set (Thermofisher Inc). The following antibodies were used to detect intracellular cytokines: IL-17A-APC (clone TC11-18H10.1, BioLegend); IFNγ-Pacific Blue (clone XMG1.2, BioLegend); Foxp3-PE (clone FJK16s, Thermofisher Scientific Inc.); in permeabilization buffer (eBioscience). Data were acquired using NovoCyte flow cytometer (ACEA Biosciences) and analyzed using FlowJo.

T-cell preparation for live cell imaging

Cd4 T cells were activated by plating on 6 well plates coated overnight with 2.5 μg/mL αCd3/αCd28 (Invivogen, San Diego, CA) at 4º C. Cells were cultured in RPMI medium (Lonza) containing 10% FCS, L-glutamine, Non-essential amino acids, Sodium pyruvate, β-mercaptoethanol and 50 U/mL of IL-2 at 37º C in 5% CO_2 incubator. Following 2 days of culture, cells were plated on either poly-L-lysine or 1 μg/mL α-Cd3/α28 coated 35mm glass chambers (Lab-Tek, Thermofisher Inc.) for imaging. RPMI medium with 2% FCS and L-glutamine containing 2 mM Ca^{2+} was used for imaging experiments. For experiments involving calibration and characterization of the Salsa6f probe in Cd4-Salsa6f cells, Ringer solution containing various concentrations of Ca^{2+} was used. For Ca^{2+} imaging of different T cell subsets, Th17 cells and iTregs were differentiated as described above.

Confocal imaging and analysis

For Ca^{2+} imaging of $Cd4^+$ T cells from Cd4-Salsa6f mice, we used an Olympus Fluoview FV3000RS confocal laser scanning microscope, equipped with high speed resonance scanner and the IX3-ZDC2 Z-drift compensator (Olympus Corp., Waltham, MA). Diode lasers (488 and 561 nm) were used for excitation, and two high-sensitivity cooled GaAsP PMTs were used for detection. Cells were imaged using the Olympus 40x silicone oil objective (NA 1.25), by taking 5 slice z-stacks at 2 µm/step, at 5 sec intervals, for up to 20 min. Temperature, humidity, and CO_2 were maintained using a Tokai-Hit WSKM-F1 stagetop incubator. Data were processed and analyzed using Imaris and ImageJ software. Calcium imaging experiments were done at 37º C on 2 day-activated $Cd4^+$ T cells from Cd4-Salsa6f (Het) mice, unless otherwise indicated. Salsa6f calibration experiments were done at room temperature.

Two-photon microscopy

Lymph nodes images were acquired using a custom-built two photon microscope based on Olympus BX51 upright frame, Motorized ZDeck stage (Prior, Rockland, MA), with excitation generated by a tunable Chameleon femtosecond laser (Coherent, Santa Clara, CA) (Miller, Wei et al. 2002). The following wavelengths were used to excite single or combination of fluorophores: 920 nm to excite tdTomato and GCaMP6f; 1040 nm to excite tdTomato alone. 495 nm and 538 nm dichroic filters were arranged in series to separate blue, green and red signals. Two-photon excitation maxima of tdTomato and GCaMP6f are 1040 and 920 nm, respectively (Drobizhev, Makarov et al. 2011, Chen, Wardill et al. 2013). Using 1040 nm excitation, tdTomato signals were readily detected up to 300 µm depth; however, 1040 is not ideal to image Salsa6f

because: 1) Collagen fibers generate second harmonic at 520 nm when excited with 1040 nm, which interferes with simultaneous detection of GCaMP6f (emission maxima, 509 nm); and 2) 1040 nm does not excite GCaMP6f (**Figure 9-figure supplement 1A, top row**). Alternatively, 920 nm optimally excites GCaMP6f, and excites tdTomato sufficiently, and Salsa6f signals were detected up to 300 µm depth, while second harmonic collagen signals (460 nm) can be easily separated into blue channel (**Figure 9-figure supplement 1A, bottom row**). Additionally, autofluorescent structures (LN resident DCs and fibroblastic reticular cells) show up as yellow bodies when excited with 920 nm, which serve as a guide to locate the T cell zone (**Figure 9-figure supplement 1B**). Therefore, 920 nm is the ideal two-photon excitation wavelength for simultaneous imaging of tdTomato and GCaMP6f as component parts of Salsa6f.

Lymph nodes were oriented with the hilum away from the water dipping microscope objective (Nikon 25x, NA 1.05). The node was maintained at 36-37℃ by perfusion with medium (RPMI) bubbled with medical grade carbogen (95% O_2 and 5% CO_2) using a peristaltic heated perfusion system (Warner Instruments), with thermocouple-based temperature sensors placed next to the tissue in a custom built chamber. 3D image stacks of x=250 µm, y=250 µm, and z=20 or 52 µm (4 µm step size) were sequentially acquired at 5 or 11 second intervals respectively, using image acquisition software Slidebook (Intelligent Imaging Innovations) as described previously (Matheu, Othy et al. 2015). This volume collection was repeated for up to 40 min to create a 4D data set.

Data analysis and statistical testing

Graphpad Prism was used for statistical analysis and generating figures. p values are indicated in figures: ns $p > 0.05$, * $p < 0.05$; ** $p < 0.01$; *** $p < 0.001$; and **** $p < 0.0001$.

Detection of Ca^{2+} signals in lymph nodes

Stacks of 6 optical sections 4 µm apart from the T-zone of Cd4-Salsa6f (Hom) lymph nodes were acquired once every 5 sec at a resolution of 0.488 or 0.684 µm per pixel. Maximum intensity projections of 1 pixel radius median-filtered images were used for subsequent processing and analysis. Autofluorescent cells were identified by averaging the red or green time lapse image stacks and automated local thresholding (Bernsen 5 pixel radius) using the public domain image processing program ImageJ. Autofluorescent cell masks were dilated by 4 pixels, regions exhibiting less contrast and detail due to light scattering manually masked to produce the final time lapse image mask. Red (tdTomato) channel fluorescence from Salsa6f corresponding to green (GCaMP6f) channel resting state fluorescence was determined to be 5-fold higher using our standard 2-photon microscope acquisition settings. Final green images were produced by subtracting a 0.2x scaled red channel image, and subsequently subtracting out the average of all green channel time lapse images. The standard deviation (SD) of each masked green channel time lapse image stack was used to determine thresholds for local (sparkle) and cell-wide Ca^{2+} events. Thresholds for detection of local and cell-wide Ca^{2+} events were 5.4 and 2.1 SD and 1.4 μm^2 and 25 μm^2, respectively. Local Ca^{2+} events were excluded from the set of sparkles if they coincided with a cell-wide event. Frequency of background events was calculated using a standard normal distribution with a Z-score corresponding to the average intensity of local events (6.5

632 SD), which was 1 in $2x10^{10}$ pixels (WolframAlpha). The front and back of motile T cells
633 were traced manually from red channel TdTomato images. Individual pixel intensities
634 from the front and back regions of interest were plotted and compared using the non-
635 parametric Mann Whitney test in Graphpad Prism.

636

References

Akerboom, J., N. Carreras Calderon, L. Tian, S. Wabnig, M. Prigge, J. Tolo, A. Gordus, M. B. Orger, K. E. Severi, J. J. Macklin, R. Patel, S. R. Pulver, T. J. Wardill, E. Fischer, C. Schuler, T. W. Chen, K. S. Sarkisyan, J. S. Marvin, C. I. Bargmann, D. S. Kim, S. Kugler, L. Lagnado, P. Hegemann, A. Gottschalk, E. R. Schreiter and L. L. Looger (2013). "Genetically encoded calcium indicators for multi-color neural activity imaging and combination with optogenetics." Front Mol Neurosci **6**: 2.

Akerboom, J., T. W. Chen, T. J. Wardill, L. Tian, J. S. Marvin, S. Mutlu, N. C. Calderon, F. Esposti, B. G. Borghuis, X. R. Sun, A. Gordus, M. B. Orger, R. Portugues, F. Engert, J. J. Macklin, A. Filosa, A. Aggarwal, R. A. Kerr, R. Takagi, S. Kracun, E. Shigetomi, B. S. Khakh, H. Baier, L. Lagnado, S. S. Wang, C. I. Bargmann, B. E. Kimmel, V. Jayaraman, K. Svoboda, D. S. Kim, E. R. Schreiter and L. L. Looger (2012). "Optimization of a GCaMP calcium indicator for neural activity imaging." J Neurosci **32**(40): 13819-13840.

Badura, A., X. R. Sun, A. Giovannucci, L. A. Lynch and S. S. Wang (2014). "Fast calcium sensor proteins for monitoring neural activity." Neurophotonics **1**(2): 025008.

Baird, G. S., D. A. Zacharias and R. Y. Tsien (1999). "Circular permutation and receptor insertion within green fluorescent proteins." Proc Natl Acad Sci U S A **96**(20): 11241-11246.

Berridge, M. J. (2012). "Calcium signalling remodelling and disease." Biochem Soc Trans **40**(2): 297-309.

Berridge, M. J., P. Lipp and M. D. Bootman (2000). "The versatility and universality of calcium signalling." Nat Rev Mol Cell Biol **1**(1): 11-21.

Cahalan, M. D. and K. G. Chandy (2009). "The functional network of ion channels in T lymphocytes." Immunol Rev **231**(1): 59-87.

Chen, L. and D. B. Flies (2013). "Molecular mechanisms of T cell co-stimulation and co-inhibition." Nat Rev Immunol **13**(4): 227-242.

Chen, T. W., T. J. Wardill, Y. Sun, S. R. Pulver, S. L. Renninger, A. Baohan, E. R. Schreiter, R. A. Kerr, M. B. Orger, V. Jayaraman, L. L. Looger, K. Svoboda and D. S. Kim (2013). "Ultrasensitive fluorescent proteins for imaging neuronal activity." Nature **499**(7458): 295-300.

Cho, J. H., C. J. Swanson, J. Chen, A. Li, L. G. Lippert, S. E. Boye, K. Rose, S. Sivaramakrishnan, C. M. Chuong and R. H. Chow (2017). "The GCaMP-R Family of Genetically Encoded Ratiometric Calcium Indicators." ACS Chem Biol **12**(4): 1066-1074.

Clapham, D. E. (2007). "Calcium signaling." Cell **131**(6): 1047-1058.

Direnberger, S., M. Mues, V. Micale, C. T. Wotjak, S. Dietzel, M. Schubert, A. Scharr, S. Hassan, C. Wahl-Schott, M. Biel, G. Krishnamoorthy and O. Griesbeck (2012). "Biocompatibility of a genetically encoded calcium indicator in a transgenic mouse model." Nat Commun **3**: 1031.

Dolmetsch, R. E. and R. S. Lewis (1994). "Signaling between intracellular Ca2+ stores and depletion-activated Ca2+ channels generates [Ca2+]i oscillations in T lymphocytes." J Gen Physiol **103**(3): 365-388.

Dong, T. X., S. Othy, M. L. Greenberg, A. Jairaman, C. Akunwafo, S. Leverrier, Y. Yu, I. Parker, J. L. Dynes and M. D. Cahalan (2017). "Intermittent Ca2+ signals mediated by Orai1 regulate basal T cell motility." Elife **6**.

Drobizhev, M., N. S. Makarov, S. E. Tillo, T. E. Hughes and A. Rebane (2011). "Two-photon absorption properties of fluorescent proteins." Nat Methods **8**(5): 393-399.

Dynes, J. L., A. Amcheslavsky and M. D. Cahalan (2016). "Genetically targeted single-channel optical recording reveals multiple Orai1 gating states and oscillations in calcium influx." Proc Natl Acad Sci U S A **113**(2): 440-445.

Gee, J. M., N. A. Smith, F. R. Fernandez, M. N. Economo, D. Brunert, M. Rothermel, S. C. Morris, A. Talbot, S. Palumbos, J. M. Ichida, J. D. Shepherd, P. J. West, M. Wachowiak, M. R. Capecchi, K. S. Wilcox, J. A. White and P. Tvrdik (2014). "Imaging Activity in Neurons and Glia with a Polr2a-Based and Cre-Dependent GCaMP5G-IRES-tdTomato Reporter Mouse." Neuron **83**(5): 1058-1072.

683 Grynkiewicz, G., M. Poenie and R. Y. Tsien (1985). "A new generation of Ca2+ indicators with greatly
684 improved fluorescence properties." J Biol Chem **260**(6): 3440-3450.
685 Hasan, M. T., R. W. Friedrich, T. Euler, M. E. Larkum, G. Giese, M. Both, J. Duebel, J. Waters, H. Bujard, O.
686 Griesbeck, R. Y. Tsien, T. Nagai, A. Miyawaki and W. Denk (2004). "Functional fluorescent Ca2+ indicator
687 proteins in transgenic mice under TET control." PLoS Biol **2**(6): e163.
688 Heim, N., O. Garaschuk, M. W. Friedrich, M. Mank, R. I. Milos, Y. Kovalchuk, A. Konnerth and O.
689 Griesbeck (2007). "Improved calcium imaging in transgenic mice expressing a troponin C-based
690 biosensor." Nat Methods **4**(2): 127-129.
691 Heim, N. and O. Griesbeck (2004). "Genetically encoded indicators of cellular calcium dynamics based on
692 troponin C and green fluorescent protein." J Biol Chem **279**(14): 14280-14286.
693 Ji, G., M. E. Feldman, K. Y. Deng, K. S. Greene, J. Wilson, J. C. Lee, R. C. Johnston, M. Rishniw, Y. Tallini, J.
694 Zhang, W. G. Wier, M. P. Blaustein, H. B. Xin, J. Nakai and M. I. Kotlikoff (2004). "Ca2+-sensing transgenic
695 mice: postsynaptic signaling in smooth muscle." J Biol Chem **279**(20): 21461-21468.
696 Krummel, M. F., F. Bartumeus and A. Gerard (2016). "T cell migration, search strategies and
697 mechanisms." Nat Rev Immunol **16**(3): 193-201.
698 Kubo, F., B. Hablitzel, M. Dal Maschio, W. Driever, H. Baier and A. B. Arrenberg (2014). "Functional
699 architecture of an optic flow-responsive area that drives horizontal eye movements in zebrafish."
700 Neuron **81**(6): 1344-1359.
701 Le Borgne, M., S. Raju, B. H. Zinselmeyer, V. T. Le, J. Li, Y. Wang, M. J. Miller and A. S. Shaw (2016). "Real-
702 Time Analysis of Calcium Signals during the Early Phase of T Cell Activation Using a Genetically Encoded
703 Calcium Biosensor." J Immunol **196**(4): 1471-1479.
704 Lewis, R. S. and M. D. Cahalan (1989). "Mitogen-induced oscillations of cytosolic Ca2+ and
705 transmembrane Ca2+ current in human leukemic T cells." Cell Regul **1**(1): 99-112.
706 Liu, D., H. Xu, C. Shih, Z. Wan, X. Ma, W. Ma, D. Luo and H. Qi (2015). "T-B-cell entanglement and ICOSL-
707 driven feed-forward regulation of germinal centre reaction." Nature **517**(7533): 214-218.
708 Lobbestael E, R. V., Ibrahimi A, Paesen K, Thiry I, Gijsbers R, Van den Haute C, Debyser Z, Baekelandt V,
709 Taymans JM. (2010). "Immunohistochemical detection of transgene expression in the brain using small
710 epitope tags." BMC Biotechnol.
711 Madisen, L., T. A. Zwingman, S. M. Sunkin, S. W. Oh, H. A. Zariwala, H. Gu, L. L. Ng, R. D. Palmiter, M. J.
712 Hawrylycz, A. R. Jones, E. S. Lein and H. Zeng (2010). "A robust and high-throughput Cre reporting and
713 characterization system for the whole mouse brain." Nat Neurosci **13**(1): 133-140.
714 Mank, M., D. F. Reiff, N. Heim, M. W. Friedrich, A. Borst and O. Griesbeck (2006). "A FRET-based calcium
715 biosensor with fast signal kinetics and high fluorescence change." Biophys J **90**(5): 1790-1796.
716 Mank, M., A. F. Santos, S. Direnberger, T. D. Mrsic-Flogel, S. B. Hofer, V. Stein, T. Hendel, D. F. Reiff, C.
717 Levelt, A. Borst, T. Bonhoeffer, M. Hubener and O. Griesbeck (2008). "A genetically encoded calcium
718 indicator for chronic in vivo two-photon imaging." Nat Methods **5**(9): 805-811.
719 Matheu, M. P., S. Othy, M. L. Greenberg, T. X. Dong, M. Schuijs, K. Deswarte, H. Hammad, B. N.
720 Lambrecht, I. Parker and M. D. Cahalan (2015). "Imaging regulatory T cell dynamics and CTLA4-mediated
721 suppression of T cell priming." Nat Commun **6**: 6219.
722 Miller, M. J., S. H. Wei, I. Parker and M. D. Cahalan (2002). "Two-photon imaging of lymphocyte motility
723 and antigen response in intact lymph node." Science **296**(5574): 1869-1873.
724 Miyawaki, A., J. Llopis, R. Heim, J. M. McCaffery, J. A. Adams, M. Ikura and R. Y. Tsien (1997).
725 "Fluorescent indicators for Ca2+ based on green fluorescent proteins and calmodulin." Nature
726 **388**(6645): 882-887.
727 Mrass, P., J. Petravic, M. P. Davenport and W. Weninger (2010). "Cell-autonomous and environmental
728 contributions to the interstitial migration of T cells." Semin Immunopathol **32**(3): 257-274.

729 Nagai, T., S. Yamada, T. Tominaga, M. Ichikawa and A. Miyawaki (2004). "Expanded dynamic range of
730 fluorescent indicators for Ca(2+) by circularly permuted yellow fluorescent proteins." Proc Natl Acad Sci
731 U S A **101**(29): 10554-10559.
732 Nakai, J., M. Ohkura and K. Imoto (2001). "A high signal-to-noise Ca(2+) probe composed of a single
733 green fluorescent protein." Nat Biotechnol **19**(2): 137-141.
734 Nourse, J. L. and M. M. Pathak (2017). "How cells channel their stress: Interplay between Piezo1 and the
735 cytoskeleton." Semin Cell Dev Biol.
736 Palmer, A. E., M. Giacomello, T. Kortemme, S. A. Hires, V. Lev-Ram, D. Baker and R. Y. Tsien (2006).
737 "Ca2+ indicators based on computationally redesigned calmodulin-peptide pairs." Chem Biol **13**(5): 521-
738 530.
739 Perez Koldenkova, V. and T. Nagai (2013). "Genetically encoded Ca(2+) indicators: properties and
740 evaluation." Biochim Biophys Acta **1833**(7): 1787-1797.
741 Portugues, R., C. E. Feierstein, F. Engert and M. B. Orger (2014). "Whole-brain activity maps reveal
742 stereotyped, distributed networks for visuomotor behavior." Neuron **81**(6): 1328-1343.
743 Prakriya, M. and R. S. Lewis (2015). "Store-Operated Calcium Channels." Physiol Rev **95**(4): 1383-1436.
744 Romoser, V. A., P. M. Hinkle and A. Persechini (1997). "Detection in living cells of Ca2+-dependent
745 changes in the fluorescence emission of an indicator composed of two green fluorescent protein
746 variants linked by a calmodulin-binding sequence. A new class of fluorescent indicators." J Biol Chem
747 **272**(20): 13270-13274.
748 Shulman, Z., A. D. Gitlin, J. S. Weinstein, B. Lainez, E. Esplugues, R. A. Flavell, J. E. Craft and M. C.
749 Nussenzweig (2014). "Dynamic signaling by T follicular helper cells during germinal center B cell
750 selection." Science **345**(6200): 1058-1062.
751 Syeda, R., J. Xu, A. E. Dubin, B. Coste, J. Mathur, T. Huynh, J. Matzen, J. Lao, D. C. Tully, I. H. Engels, H. M.
752 Petrassi, A. M. Schumacher, M. Montal, M. Bandell and A. Patapoutian (2015). "Chemical activation of
753 the mechanotransduction channel Piezo1." Elife **4**.
754 Tallini, Y. N., M. Ohkura, B. R. Choi, G. Ji, K. Imoto, R. Doran, J. Lee, P. Plan, J. Wilson, H. B. Xin, A. Sanbe,
755 J. Gulick, J. Mathai, J. Robbins, G. Salama, J. Nakai and M. I. Kotlikoff (2006). "Imaging cellular signals in
756 the heart in vivo: Cardiac expression of the high-signal Ca2+ indicator GCaMP2." Proc Natl Acad Sci U S A
757 **103**(12): 4753-4758.
758 Thestrup, T., J. Litzlbauer, I. Bartholomaus, M. Mues, L. Russo, H. Dana, Y. Kovalchuk, Y. Liang, G.
759 Kalamakis, Y. Laukat, S. Becker, G. Witte, A. Geiger, T. Allen, L. C. Rome, T. W. Chen, D. S. Kim, O.
760 Garaschuk, C. Griesinger and O. Griesbeck (2014). "Optimized ratiometric calcium sensors for functional
761 in vivo imaging of neurons and T lymphocytes." Nat Methods **11**(2): 175-182.
762 Tian, L., S. A. Hires, T. Mao, D. Huber, M. E. Chiappe, S. H. Chalasani, L. Petreanu, J. Akerboom, S. A.
763 McKinney, E. R. Schreiter, C. I. Bargmann, V. Jayaraman, K. Svoboda and L. L. Looger (2009). "Imaging
764 neural activity in worms, flies and mice with improved GCaMP calcium indicators." Nat Methods **6**(12):
765 875-881.
766 Tsien, R. Y., T. Pozzan and T. J. Rink (1982). "Calcium homeostasis in intact lymphocytes: cytoplasmic free
767 calcium monitored with a new, intracellularly trapped fluorescent indicator." J Cell Biol **94**(2): 325-334.
768 Turley, S. J., A. L. Fletcher and K. G. Elpek (2010). "The stromal and haematopoietic antigen-presenting
769 cells that reside in secondary lymphoid organs." Nat Rev Immunol **10**(12): 813-825.
770 Vremec, D., J. Pooley, H. Hochrein, L. Wu and K. Shortman (2000). "CD4 and CD8 expression by dendritic
771 cell subtypes in mouse thymus and spleen." J Immunol **164**(6): 2978-2986.
772 Yosef, N., A. K. Shalek, J. T. Gaublomme, H. Jin, Y. Lee, A. Awasthi, C. Wu, K. Karwacz, S. Xiao, M. Jorgolli,
773 D. Gennert, R. Satija, A. Shakya, D. Y. Lu, J. J. Trombetta, M. R. Pillai, P. J. Ratcliffe, M. L. Coleman, M. Bix,
774 D. Tantin, H. Park, V. K. Kuchroo and A. Regev (2013). "Dynamic regulatory network controlling TH17 cell
775 differentiation." Nature **496**(7446): 461-468.

776 Zariwala, H. A., B. G. Borghuis, T. M. Hoogland, L. Madisen, L. Tian, C. I. De Zeeuw, H. Zeng, L. L. Looger,
777 K. Svoboda and T. W. Chen (2012). "A Cre-dependent GCaMP3 reporter mouse for neuronal imaging in
778 vivo." J Neurosci **32**(9): 3131-3141.
779 Zhang, R. D. and E. E. Henderson (1994). "CD4 mRNA expression in CD19-positive B cells and its
780 suppression by the Epstein-Barr virus." Virology **198**(2): 709-713.
781 Zhao, Y., S. Araki, J. Wu, T. Teramoto, Y. F. Chang, M. Nakano, A. S. Abdelfattah, M. Fujiwara, T. Ishihara,
782 T. Nagai and R. E. Campbell (2011). "An expanded palette of genetically encoded Ca(2)(+) indicators."
783 Science **333**(6051): 1888-1891.

784

Figure Legends

Figure 1. **Design of novel tdTomato-V5-GCaMP6f fusion probe "Salsa6f" and characterization in living cells.** (**A**) Several genetically encoded Ca^{2+} indicators were screened in vitro in HEK 293A cells, by co-transfecting with Orai1/STIM1 and measuring Ca^{2+} influx after thapsigargin-induced store depletion. Bars indicate maximum change in fluorescence intensity (dark) and dynamic range (DR: light) with Salsa6f shown in orange bars on right; n > 30 cells per probe, from two different transfections, error bars indicate SEM. (**B**) Diagram of Salsa6f construct used in transfection. (**C**) Averaged thapsigargin-induced Ca^{2+} entry, measured by change in green fluorescence, in GCaMP6f- (green, 11.5 ± 0.3, n = 63) or Salsa6f- (orange, 10.2 ± 0.3, n = 78) transfected HEK cells; data from two different transfections, error bars indicate SEM. (**D**) Two-photon images of Salsa6f co-transfected in HEK cells with Orai1/STIM1, showing red (tdTomato), green (GCaMP6f), and merged channels, at baseline in 0 mM extracellular Ca^{2+} (top) and after maximum stimulation with 2 µM ionomycin in 2 mM extracellular Ca^{2+} (bottom); scale bar = 20 µm; see **Video 1**; data are representative of at least three different experiments. (**E**) Confocal time lapse microscopy of human $Cd4^{+}$ T cells previously transfected with Salsa6f and then activated for two days on plate-bound αCd3/28 antibodies; time = min:sec, scale bar = 10 µm. (**F**) Representative traces of green fluorescence intensity from individual activated human T cells transfected with Salsa6f. Data are representative of at least three different experiments.

Figure 2. Generation of a Salsa6f transgenic mouse line targeted to the Rosa26 locus. (**A**) Transgenic targeting vector for Salsa6f, inserted between Rosa26 homology arms and electroporated into embryonic stem cells. CAG Pr: cytomegalovirus early enhancer/chicken β-actin promoter; Salsa6f: tdTomato-V5-GCaMP6f; FRT, LoxP, AttB, AttP: recombinase sites; WPRE: woodchuck hepatitis virus posttranscriptional regulatory element; pA: bovine growth hormone polyadenylation sequence; NeoR: neomycin resistance gene. (**B**) Correctly targeted ES cells were screened by Southern blot after HindIII digest for the 5' end (top) or BglI digest for the 3' end (bottom). The two clones marked in red failed to integrate at the 5' end. (**C**) PCR screening for chimeras based on presence of the Nnt mutation, present only in JM8.N4 ES cells but not in the

C57BL/6J blastocyst donors. 2540 and 2543 are chimeras. Control lanes on the right are wildtype (*Nnt*$^{+/+}$), heterozygous (*Nnt*$^{+/-}$), or homozygous mutant (*Nnt*$^{-/-}$).

Figure 3. Cd4-Salsa6f mice show normal immune cell development and expression. (**A**) Experimental design to target expression of Salsa6f in Cd4 cells. (**B**) Cd4, Cd8 and double-positive cells gated on tdTomato (Salsa6f^{+} cells) from thymus. (**C**) Histograms showing percent of Salsa6f^{+} cells in spleen, LN, and thymus. (**D**) Cd4, Cd8, and double positive cells from spleen, gated on tdTomato (Salsa6f^{+} cells). (**E**) Histograms showing percent of Salsa6f^{+} cells within Cd4, Cd8, Cd19, Cd11b populations from spleen. (**F**) Total number of Cd4, Cd8, Cd19, Cd11b cells in the spleen of Cd4-Salsa6f (Het) mice and *Cd4*^{Cre} mice (n=6 mice). (**G**) Relative percentages of Cd4, Cd8, Cd19, Cd11b cells in thymus, lymph nodes, and spleen of Cd4-Salsa6f mice and *Cd4*^{Cre} mice (n=6).

Figure 4. Functional responses of Cd4-Salsa6f T cells in vitro. (**A**) Representative histogram showing cell trace violet (CTV) dilution in *Cd4*^{Cre} (dark grey), Cd4-Salsa6f (Het) (blue), and Cd4-Salsa6f (Hom) (red) T cells at 72 hr following stimulation with αCd3/28 Dynabeads (1:1 ratio). (**B**) Proliferation index measured on CTV dilution curves (n=8). (**C-E**) Dot plots showing differentiation of naive T cells from *Cd4*^{Cre} and Cd4-Salsa6f (Het) mice into Th1 cells (**C**), Th17 cells (**D**) and iTregs (**E**) after 6 days (n = 4 mice). Right panels show average percentages of IFNγ^{+} cells (**C**)**,** IL-17^{+} cells (**D**) and Foxp3^{+} cells (**E**).

Figure 4-supplement 1. Differentiation of Cd4-Salsa6f (Hom) T cells into Th1 and iTregs. Representative dot plots showing differentiation of Cd4^{+} T cells from *Cd4*^{Cre} and Cd4-Salsa6f (Hom) mice into Th1 cells (top panel) and iTregs (bottom panel) after 4 day of stimulation with αCd3/28 Dynabeads (1:1 ratio) in the presence of polarizing cytokines. Numbers inside the plots indicate percent of cells in respective gates (mean ± SD, n=4).

Figure 5. Single-cell Salsa6f calcium signals in T cells. (**A**) Confocal images of Ca^{2+} signals in activating Cd4^{+} T cells from Cd4-Salsa6f (Het) mice, after two day stimulation on plate bound αCd3/28 antibody, showing merged green (GCaMP6f) and red (tdTomato) channels; time = min:sec; scale bar = 10 μm. (**B**) Representative traces from

cell #3 in (**A**), showing cell-wide fluorescence intensity changes in GCaMP6f (green), tdTomato (red), and green/red ratio (G/R, blue). (**C**) G/R ratios for cells 1, 2, and 4 from (**A**). (**D**) Dynamic range of Salsa6f in resting Cd4 T cells, measured as green/red fluorescence ratio by flow cytometry. Cells were pre-treated with 10 μM ionomycin in Ca^{2+}-free solution (white bar), followed by re-addition of 10 mM Ca^{2+} (blue bar). (**E**) Averaged tdTomato fluorescence in resting T cells from heterozygous Cd4-Salsa6f compared to homozygotic Cd4-Salsa6f mice.

Figure 6. Probe characterization and calibration of [Ca^{2+}] in Salsa6f T cells. (**A**) Confocal images of a naïve T cell from a Cd4-Salsa6f (Het) mouse. Upper panel: tdTomato (left) and GCaMP6f (right) fluorescence intensity in Ca^{2+}-free Ringer solution. Lower panel: same cell treated with 2 μM thapsigargin (TG) in Ringer solution containing 2 mM Ca^{2+}. Line scans for each condition are shown adjacent to the images. Scale bar = 2 μm for **A-C**. (**B)** Corresponding confocal images and line scans of Salsa6f localization in a 2-day activated $Cd4^+$ T-cell from Cd4-Salsa6f (Het) mouse. **(C)** Confocal image of a Fluo-4 (5 μM) loaded $Cd4^+$ T cell from *Cd4*^{Cre} mouse. **(D)** Average GCaMP6f and tdTomato intensities in 2-day activated $Cd4^+$ T cells treated with 2 μM ionomycin in Ca^{2+} free buffer and in external Ringer solution containing 0.1, 0.3 and 1mM Ca^{2+}. n = 36 cells, representative of 3 experiments. **(E)** Average 340 / 380 nm ratios in two day-activated and fura-2 loaded $Cd4^+$ T cells from *Cd4*^{Cre} mice (n=59 cells) and G/R ratios in two day activated $Cd4^+$ T cells from Cd4-Slasa6f (Het) mice (n=47 cells) treated identically with 2 μM ionomycin followed by graded increases of external Ca^{2+} concentration as indicated. **(F)** Steady-state fura-2 and Salsa6f ratios recorded 300 s after solution application and peak Salsa6f ratio from **6E** plotted as a function of external Ca^{2+} concentration. **(G)** Steady-state and peak Salsa6f ratios plotted as a function of cytosolic Ca^{2+} concentrations calculated from the fura-2 experiment, assuming a fura-2 K_d of 225 nM. The points were fit with a 4 parameter Hill equation to obtain the K_d for Salsa6f, with the following parameters: Salsa6f steady-state: Hill coefficient = 1.49 ± 0.16; K_d = 301 ± 24; Salsa6f peak: Hill coefficient = 0.93 ± 0.4; K_d = 162 ± 48. Data are representative of three experiments.

Figure 6-supplement 1. Comparison of GECI localization in Cd4 T cells from Salsa6f mouse and PC::G5-tdT mouse. (**A,B**) Confocal images of $Cd4^+$ T cells purified from a Cd4-Salsa6f (Het) mouse (**A**) or a Cd4-5GtdT mouse (**B**), showing merged red and green; cells imaged at the same laser and PMT settings; scale bar = 10 μm. (**C,D**) $Cd4^+$ T cells purified from a Cd4-Salsa6f (Het) mouse (**C**) or a Cd4-5GtdT mouse (**D**), then activated for 24 hr on plate-bound αCd3/28 antibodies, and imaged with confocal microscopy, showing red (tdTomato), green (GCaMP6f or GCaMP5G), and merged channels; scale bar = 10 μm.

Figure 7. Ca^{2+} signals in two day activated $Cd4^+$ T cells from Cd4-Salsa6f (Het) mice in response to store-depletion, TCR stimulation and stimulation by Yoda1. In all panels, average Salsa6f G/R ratios are shown on the left, and representative single-cell traces are shown superimposed on right. Experiments were done in standard Ringer solution (**A**) or in RPMI containing 2% FCS and 2 mM Ca^{2+} (**B-D**). **(A)** Store-operated Ca^{2+} entry (SOCE) in $Cd4^+$ T cells (n = 86 cells), induced by depleting ER Ca^{2+} stores with TG in Ca^{2+}-free buffer followed by re-addition of Ringer containing 2 mM Ca^{2+}**. (B,C)** Ca^{2+} responses to TCR stimulation in T cells plated on coverslips coated with 1 μg/ml αCd3/Cd28 (**B**) or 1 μg/ml αCd3 alone (**C**) (n = 90 cells each). **(D)** Ca^{2+} elevations during shear stress induced by solution exchange followed by the Piezo1 agonist Yoda1 (15 μM) in cells plated on αCd3/28 (n = 79 cells).

Figure 7-figure supplement 1. Store-operated Ca^{2+} entry and Piezo1 activation in T cells from Cd4-Salsa6f (Het) mice. Average (left panel) and representative single cell responses (right panel) to (**A**) TG-induced SOCE in naïve T cells (n = 96 cells), (**B**) solution exchange with media alone in 2-day activated T-cells (n = 68 cells) and (**C**) application of 15 μM Yoda1 in naïve T cells (n = 53 cells).

Figure 8. TCR induced Ca^{2+} signals in T cell subsets from Cd4-Salsa6f (Het) mice. Average (left) and representative single-cell Ca^{2+} traces (right) from confocal time-lapse microscopy showing changes in Salsa6f green/red (G/R) ratio in naïve T cells (**A**), 5 day differentiated Th17 cells (**B**), and 5 day differentiated iTregs (**C**) plated on 1 μg/mL αCd3/28. (n = 90 cells from 2 - 3 experiments each).

Figure 9. Lymph nodes from Cd4-Salsa6f (Hom) mice exhibit cell-wide and subcellular Ca^{2+} signals. (**A**) Median filtered, maximum intensity projection of a red channel image from a single time point of an explanted lymph node from a Cd4-Salsa6f (Hom) mouse. (**B**) Green channel image corresponding to **A**. Orange arrowhead indicates cell-wide Ca^{2+} signal and gray arrowheads indicate smaller, local transient Ca^{2+} signals. (**C, D**) Enlargements of cell-wide (**C**) and local (**D**; gray arrowheads) Ca^{2+} signals. Note the lower fluorescence intensity in the center of the cell in C due to exclusion of Salsa6f from the nucleus. (**E**) Maximum intensity projection of 214 green channel time points (every 11.5 seconds over 41 minutes) showing hundreds of small local Ca^{2+} signals. Green channel image series was red channel subtracted and cropped from **B**. Asterisks indicate regions containing autofluorescent cells that have been cropped out. (**F, G**) Surface plot of maximum green channel intensity over two (**F**) and 50 (**G**) consecutive time points. Note the presence of four (**F**) and dozens (**G**) of small, discrete, high intensity peaks of similar intensity. (**H**) Bar graph of relative frequencies of cell-wide and local Ca^{2+} signals. (**I**) Frequency distribution of the area of local Ca^{2+} signals. Scale bar in **A** is 100 µm (applies to **B**); scale bar in **C** is 10 µm (applies to **D**), scale bars in **E** and in **F** are 50 µm (applies to **G**). (**J**) Trace of fluorescence intensity over 25 minutes at the location of a transient subcellular Ca^{2+} signal (one time point every 5 seconds). (**K**) Trace of fluorescence intensity of a putative cell process from an autofluorescent cell drifting in the image field.

Figure 9-figure supplement 1. Imaging lymph nodes of Cd4-Salsa6f homozygous mice. Cre-mediated expression of Salsa6f in Cd4 T cells reveals endogenous T cell labeling in lymph node. (**A**)Two-photon images of explanted lymph node from Cd4-Salsa6f (Hom) mouse at various depths (indicated above each frame); 1040 nm femtosecond excitation (top row) or 920 nm excitation (bottom row). Second harmonic signal from collagen fibers is collected in green for 1040 nm excitation and in blue for 920 nm excitation. Salsa6f cells are readily detected up to 275 µm deep. (**B**) Montage image of a Cd4-Salsa6f (Hom) lymph node at 100 µm depth, imaged using 920 nm excitation showing Salsa6f^{+} cells in red, autofluorescent structures in yellow, and the capsular boundary shown in blue (second-harmonic signal). B cell follicles (F) are outlined. Scale bar = 100 µm.

Figure 9-figure supplement 2. Subtraction of red channel fluorescence improves detection of Salsa6f Ca^{2+} signals. (**A, B**) Median filtered, maximum intensity projection of a red channel image from a single time point of an explanted lymph node from a Cd4-Salsa6f (Hom) mouse. Panel **A** is enlarged and cropped from panel **B** (gray rectangle). (**C, E, G**) Green channel images corresponding to **A** with different image processing protocols. (**C**) Maximum intensity projection without further processing. (**E**) Maximum intensity projection after subtraction of the average of all green channel frames. (**G**) Maximum intensity projection after subtraction of the corresponding scaled red channel image and subtraction of the subsequent average from all green channel frames. Green arrows in **C,E,G** indicate a subcellular Ca^{2+} signal. (**D, F, H**) Surface plots corresponding to the images in **C,E,G** respectively showing the subcellular Ca^{2+} signal as a green peak. Gray arrowheads indicate nearby background cell fluorescence that is progressively removed by image processing. Asterisk indicates a region containing an autofluorescent cell that has been cropped out. Scale bar in **A** is 25 µm (applies to **C,E,G**); scale bar in **B** and the horizontal scale bar in **D** are 50 µm (applies to **F,H**).

Figure 10. Subcellular Ca^{2+} signals map to different regions of motile, adoptively transferred Cd4-Salsa6f (Hom) T cells. (**A**) Histogram of green channel pixel intensities from a representative region of a time-lapse image series of Cd4-Salsa6f (Hom) T cells in a wild type lymph node after adoptive transfer. Vertical marks indicate the peak intensities of the fluorescence transients shown in **D** and **J**. (**B-F, H-L**) Two Cd4-Salsa6f (Hom) T cells imaged in a wild type lymph node after adoptive transfer (same lymph node as in **A**). Red (**B,H**) and green (**C,I**) channel fluorescence images. (**D,J**) Corresponding pseudocolored green channel images processed as in Figure 9-figure supplement 2. (**E,K**) Corresponding composite image of gray pseudocolored red channel image with green channel processed image. (**F,L**) Ratiometric images of the green divided by the red channel fluorescence image. Gray arrowheads denote local Ca^{2+} signals at the back (**C-F**) and front (**I-L**) of motile T cells. Look-up table for **D** and **J** corresponds to Arbitrary Units; look-up table for **F** and **L** corresponds to green-to-red ratio. Both cells are oriented with their front toward the top of the image. Scale bar in A is 5 µm (applies to **B-H, H-L**). (**G,M**) Scatter plots of G/R ratio for individual pixels in the

964 front and back of Cd4-Salsa6f T cells shown in **B-F** and **H-L**, respectively. Red lines
965 indicate median values. (****) indicates $p<0.0001$, Mann Whitney test.

966

Video Legends

Video 1. Calcium readout of Salsa6f probe in HEK cells. HEK 293A cells transfected with Salsa6f, first washed with 0 mM Ca^{2+} followed by 2 µM ionomycin in 2 mM Ca^{2+}; scale bar = 20 µm, time shown in hr:min:sec. Images were acquired at 15 second interval and played back at 15 frames per second. This video corresponds to **Figure 1D**.

Video 2. Single-cell readout of activation in transgenic T cells by Salsa6f. Cd4 T cells from Cd4-Salsa6f (Het) mice were plated on activating surface coated with anti-Cd3/Cd28. Images were acquired at 5 second interval and played back at 15 frames per second. This video corresponds to **Figure 5A.**

Video 3. T cell Ca^{2+} response to Ca^{2+} store depletion by thapsigargin (TG). Video of maximum intensity projection images of 2 day activated T cells from Cd4-Salsa6f (Het) mouse plated on poly-L-lysine. Scale bar = 20 µm, time shown in hr:min:sec. 2 µM TG in Ca^{2+} free Ringer's was added at 00:02:30 and 2 mM $Ca^{2+}$was added at 00:08:15. Time interval between frames is 5 sec. Play back speed = 50 frames per second. This video corresponds to **Figure 7A**.

Video 4. Activated T cell Ca^{2+} responses to TCR stimulation. Video of maximum intensity projection images of 2 day activated T cells from Cd4-Salsa6f (Het) mouse plated on anti-Cd3/28 coated coverslip. Scale bar = 20 µm, time shown in hr:min:sec. Time interval between frames is 5sec. Play back speed = 15 frames per second. Video corresponds to **Figure 7B**.

Video 5. **T cell Ca^{2+} response to shear and Yoda1.** Video of maximum intensity projection images of 2 day activated T cells from Cd4-Salsa6f (Het) mouse plated on anti-Cd3/28 coated coverslip. Scale bar = 20 µm, time shown in hr:min:sec. Time interval between frames is 5sec. Play back speed = 200 frames per second. Medium was added at 00:15:00and Yoda1 was added at 00:35:00. Video corresponds to **Figure 7C**.

Video 6. Lymph nodes from Cd4-Salsa6f (Hom) mice exhibit cell-wide and subcellular Ca^{2+} signals. Time shown in hr:min:sec; images were acquired at 5 second intervals. Play back speed = 50 frames per second. Red channel is turned off after beginning to facilitate visualization of green signals. Video corresponds to **Figure 9B.**

Figure 1

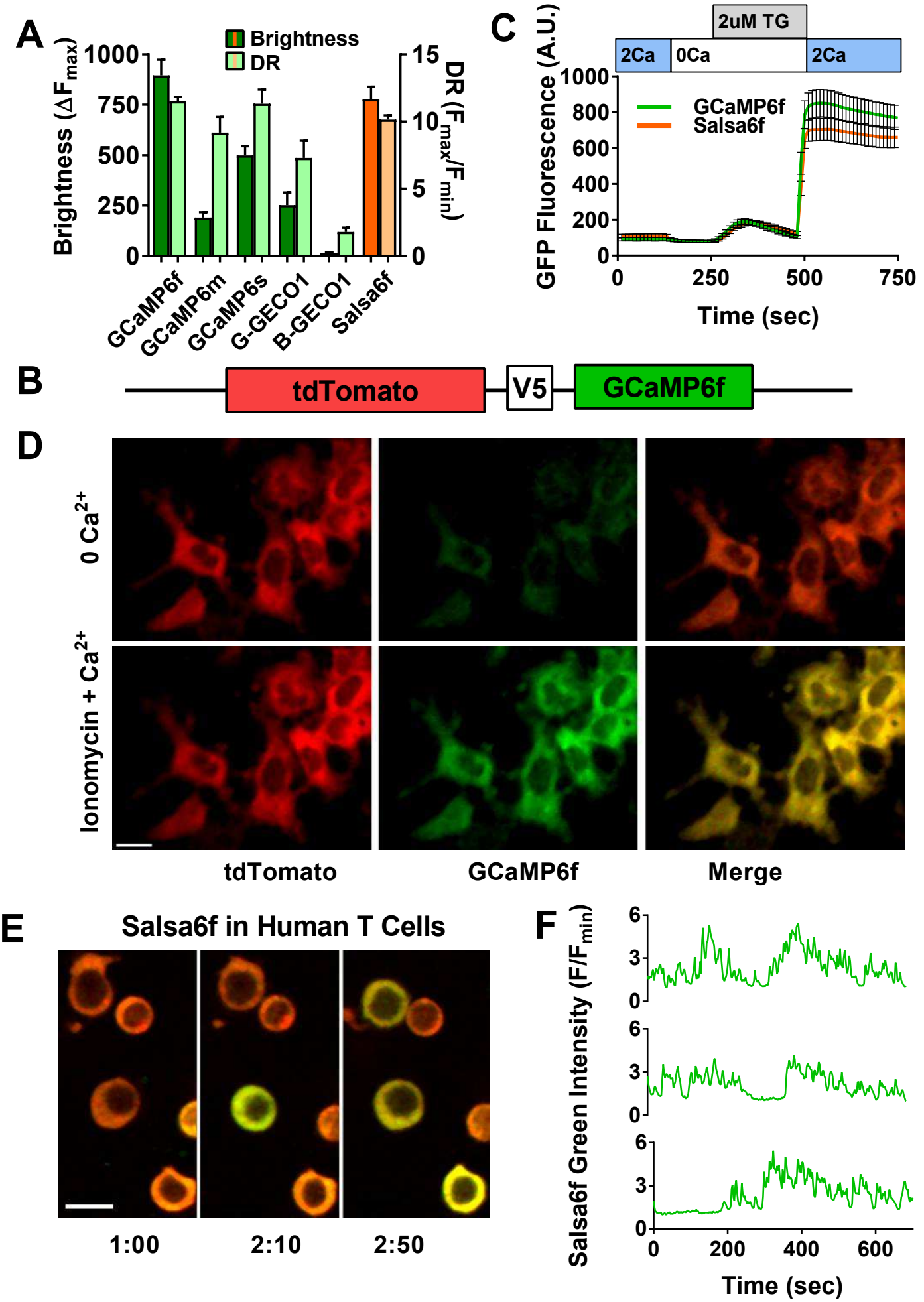
A
Brightness
DR
Brightness (ΔF_max)
DR (F_max/F_min)
1000
750
500
250
0
15
10
5
0
GCaMP6f
GCaMP6m
GCaMP6s
G-GECO1
B-GECO1
Salsa6f
C
2uM TG
2Ca
0Ca
2Ca
GCaMP6f
Salsa6f
GFP Fluorescence (A.U.)
1000
800
600
400
200
0
0
250
500
750
Time (sec)
B
tdTomato
V5
GCaMP6f
D
0 Ca2+
Ionomycin + Ca2+
tdTomato
GCaMP6f
Merge
E
Salsa6f in Human T Cells
1:00
2:10
2:50
F
Salsa6f Green Intensity (F/F_min)
6
3
0
6
3
0
6
3
0
0
200
400
600
Time (sec)

Figure 2

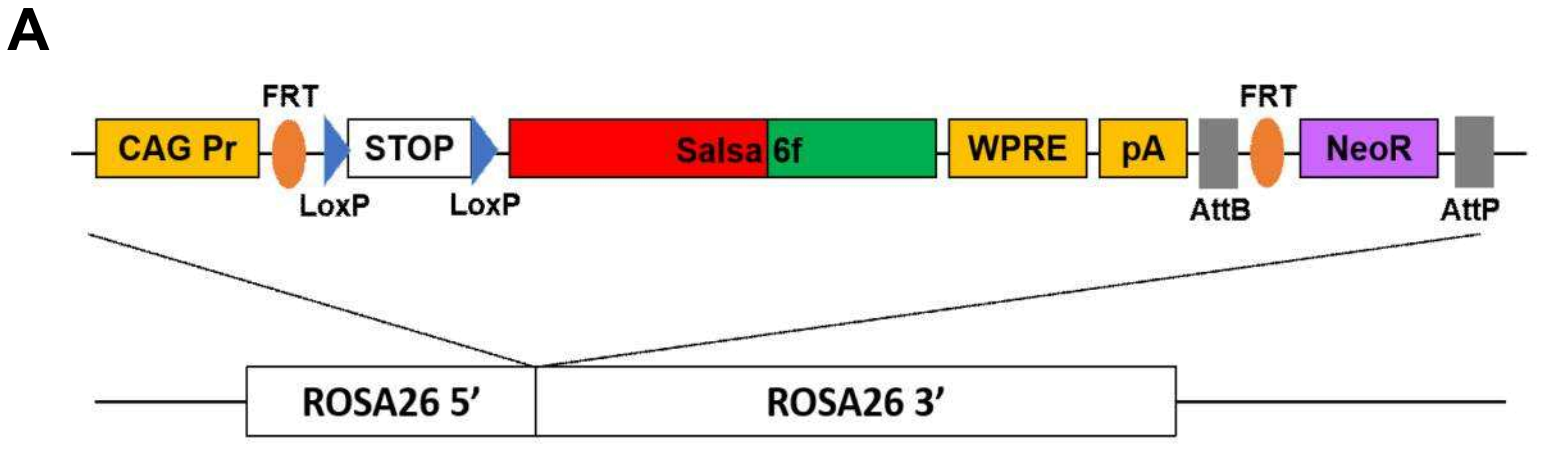
A
FRT
CAG Pr
STOP
LoxP
LoxP
Salsa 6f
WPRE
pA
FRT
NeoR
AttB
AttP
ROSA26 5'
ROSA26 3'
B
Hind III 5' probe
Targeted, 5.5 kb
Wild-type, 4.4 kb
BglI 3' probe
Targeted, 7.6 kb
Wild-type, 6.8 kb
C
2540
2541
2542
2543
2544
2545
+/+
+/-
-/-

Figure 3

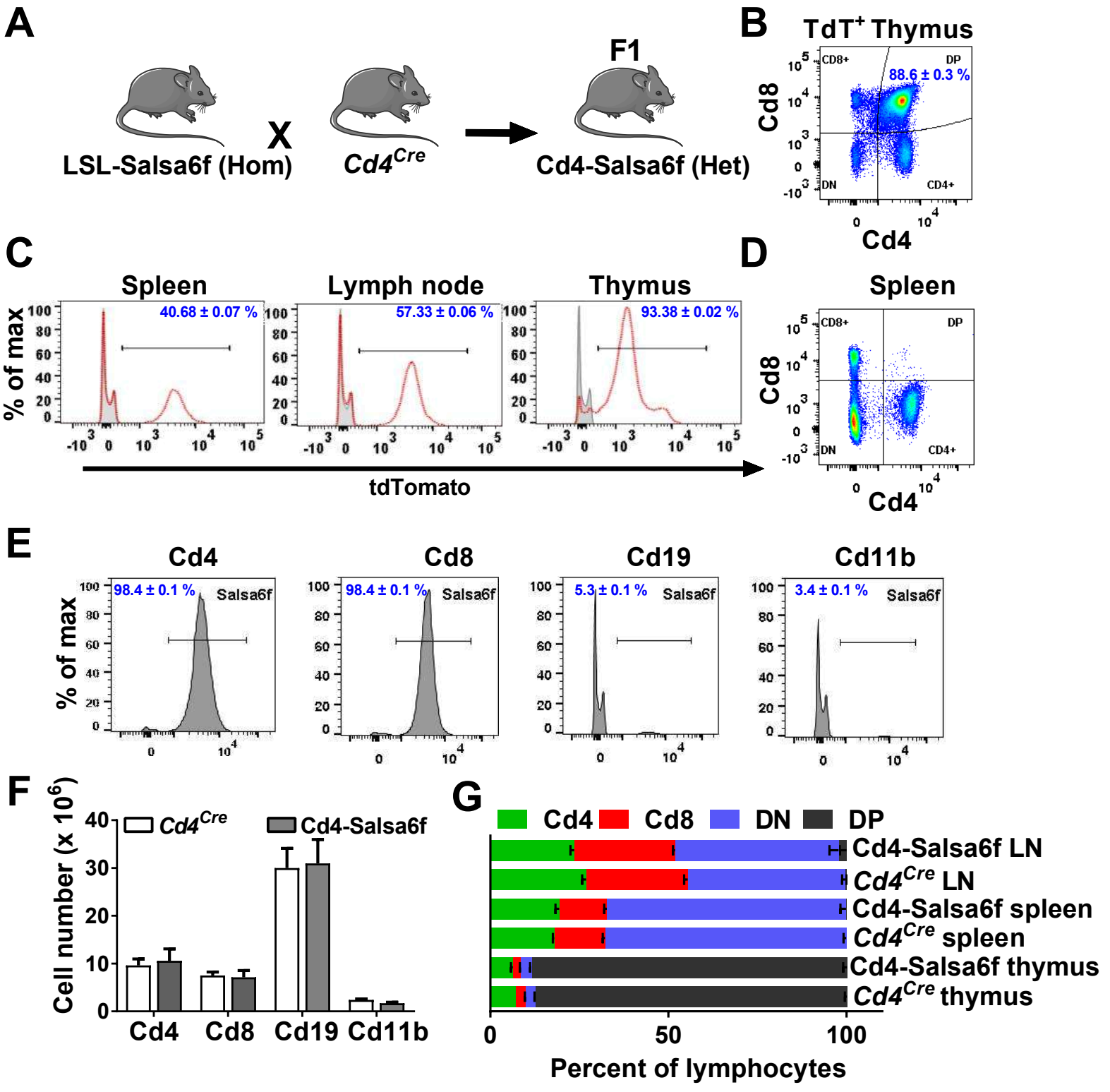
A
LSL-Salsa6f (Hom)
X
Cd4Cre
F1
Cd4-Salsa6f (Het)
B
TdT+ Thymus
CD8+
DP
88.6 ± 0.3 %
DN
CD4+
Cd8
Cd4
C
Spleen
Lymph node
Thymus
40.68 ± 0.07 %
57.33 ± 0.06 %
93.38 ± 0.02 %
% of max
tdTomato
D
Spleen
E
Cd4
Cd8
Cd19
Cd11b
98.4 ± 0.1 %
98.4 ± 0.1 %
5.3 ± 0.1 %
3.4 ± 0.1 %
Salsa6f
F
Cd4Cre
Cd4-Salsa6f
Cell number (x 10^6)
Cd4
Cd8
Cd19
Cd11b
G
Cd4
Cd8
DN
DP
Cd4-Salsa6f LN
Cd4Cre LN
Cd4-Salsa6f spleen
Cd4Cre spleen
Cd4-Salsa6f thymus
Cd4Cre thymus
Percent of lymphocytes

Figure 4

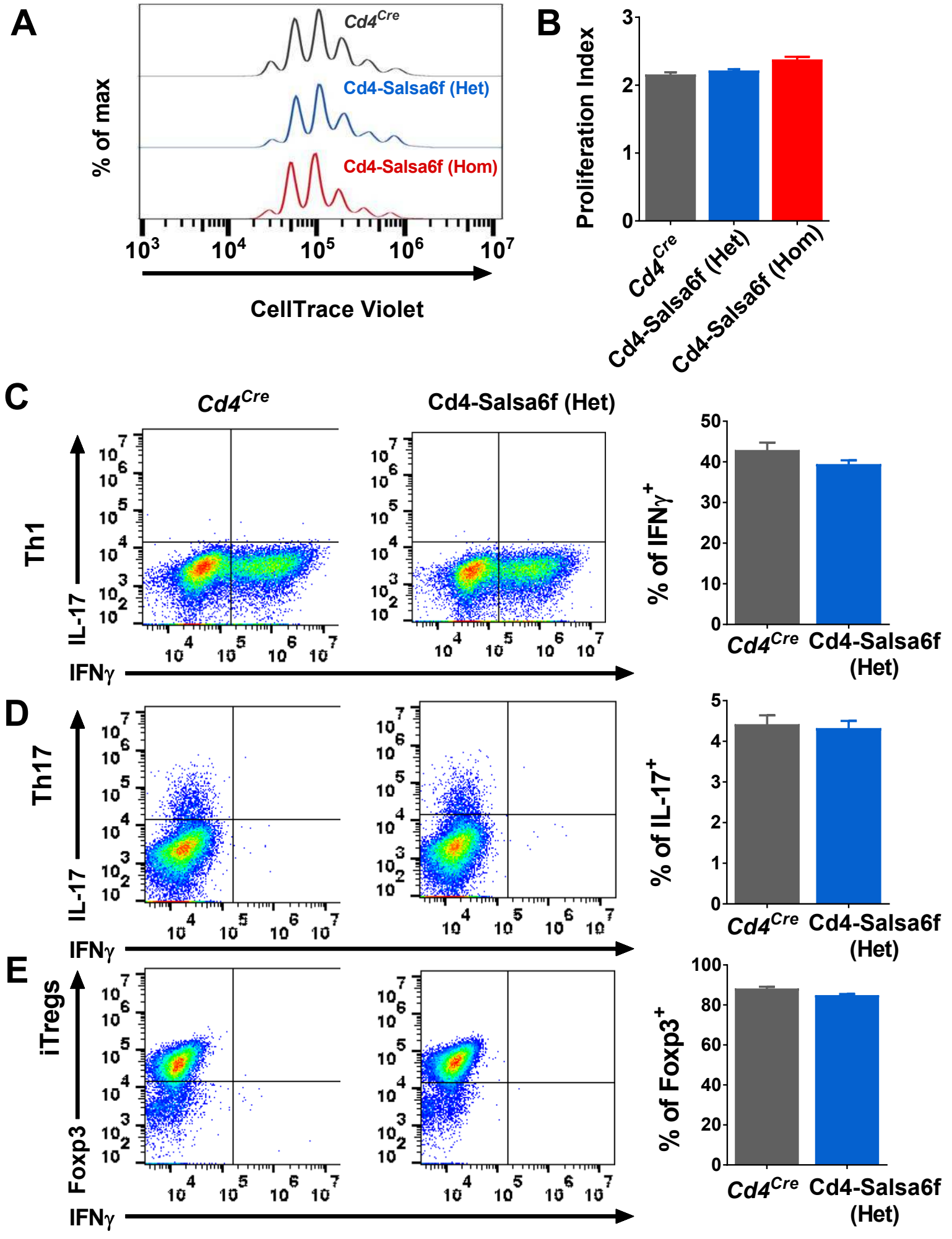
A
Cd4Cre
Cd4-Salsa6f (Het)
Cd4-Salsa6f (Hom)
% of max
CellTrace Violet
B
Proliferation Index
Cd4Cre
Cd4-Salsa6f (Het)
Cd4-Salsa6f (Hom)
C
Cd4Cre
Cd4-Salsa6f (Het)
Th1
IL-17
IFNγ
% of IFNγ+
D
Th17
IL-17
IFNγ
% of IL-17+
E
iTregs
Foxp3
IFNγ
% of Foxp3+

Figure 4 - Figure supplement 1

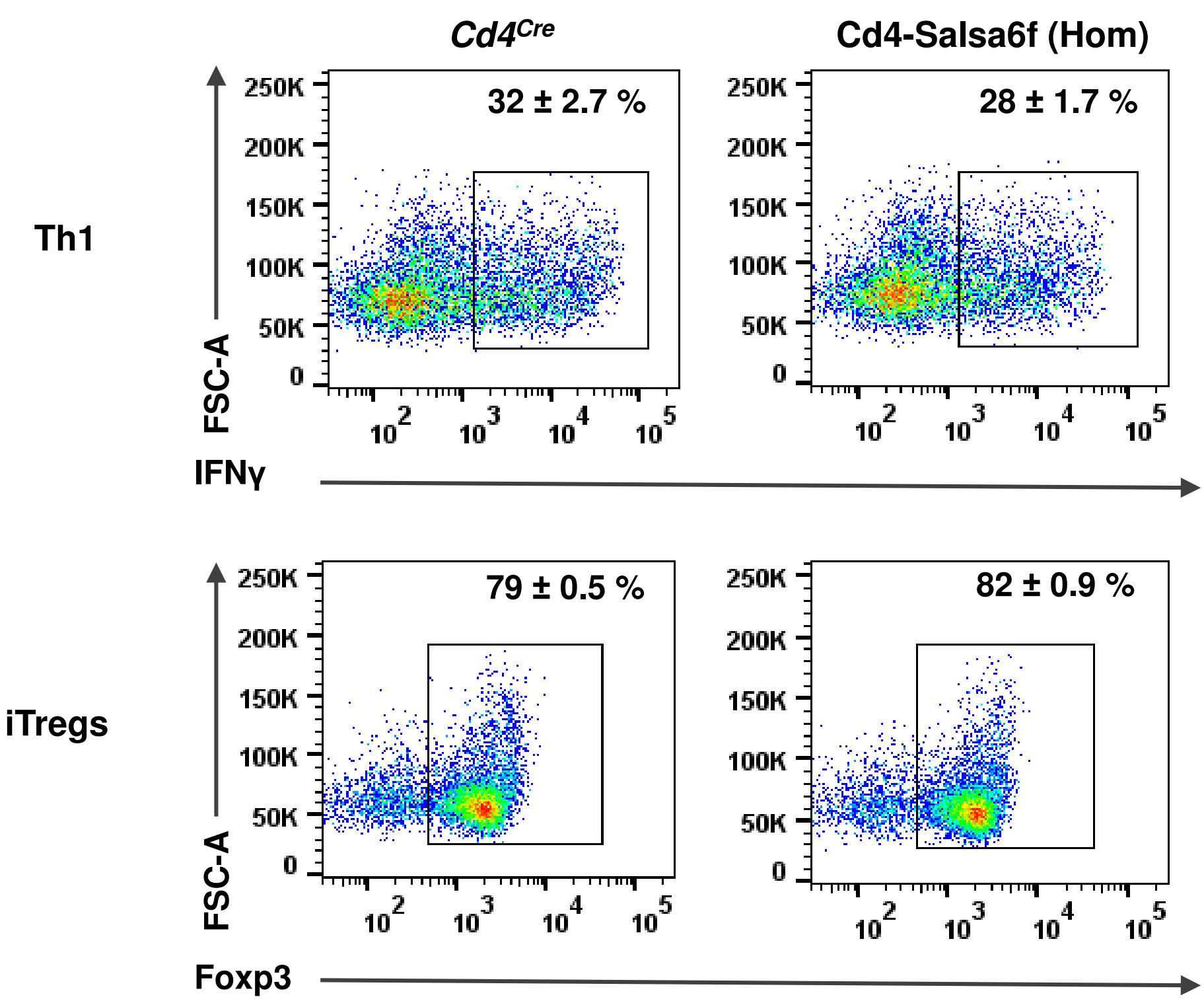

Figure 5

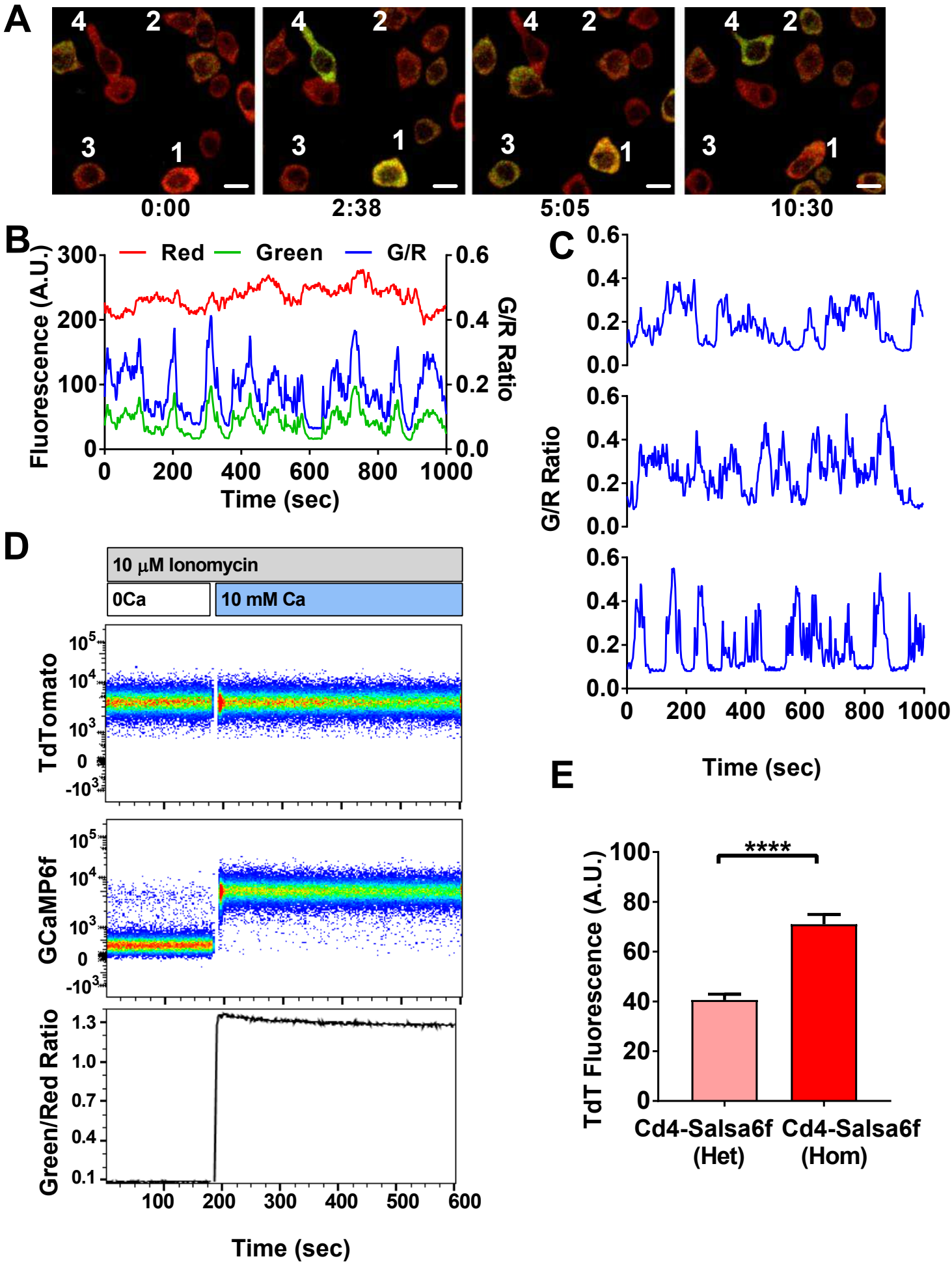
A
4
2
3
1
0:00
2:38
5:05
10:30
B
Red
Green
G/R
Fluorescence (A.U.)
G/R Ratio
Time (sec)
C
G/R Ratio
Time (sec)
D
10 μM Ionomycin
0Ca
10 mM Ca
TdTomato
GCaMP6f
Green/Red Ratio
Time (sec)
E
****
TdT Fluorescence (A.U.)
Cd4-Salsa6f (Het)
Cd4-Salsa6f (Hom)

Figure 6

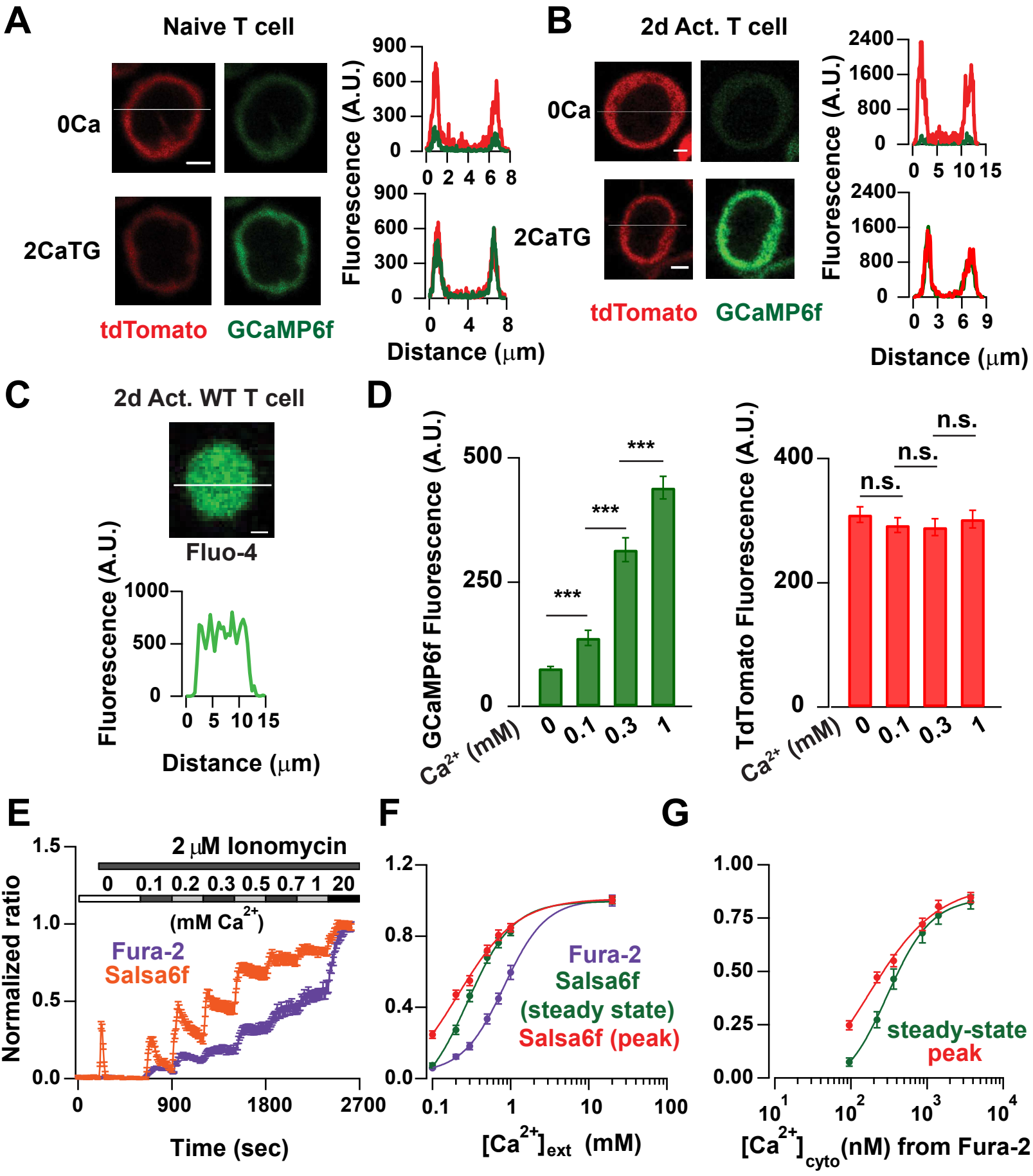
A
Naive T cell
0Ca
2CaTG
tdTomato
GCaMP6f
Fluorescence (A.U.)
Distance (μm)
B
2d Act. T cell
C
2d Act. WT T cell
Fluo-4
D
GCaMP6f Fluorescence (A.U.)
TdTomato Fluorescence (A.U.)
n.s.
***
Ca2+ (mM)
E
2 μM Ionomycin
(mM Ca2+)
Fura-2
Salsa6f
Normalized ratio
Time (sec)
F
Fura-2
Salsa6f
(steady state)
Salsa6f (peak)
[Ca2+]ext (mM)
G
steady-state
peak
[Ca2+]cyto (nM) from Fura-2

Figure 6- Figure Supplement 1

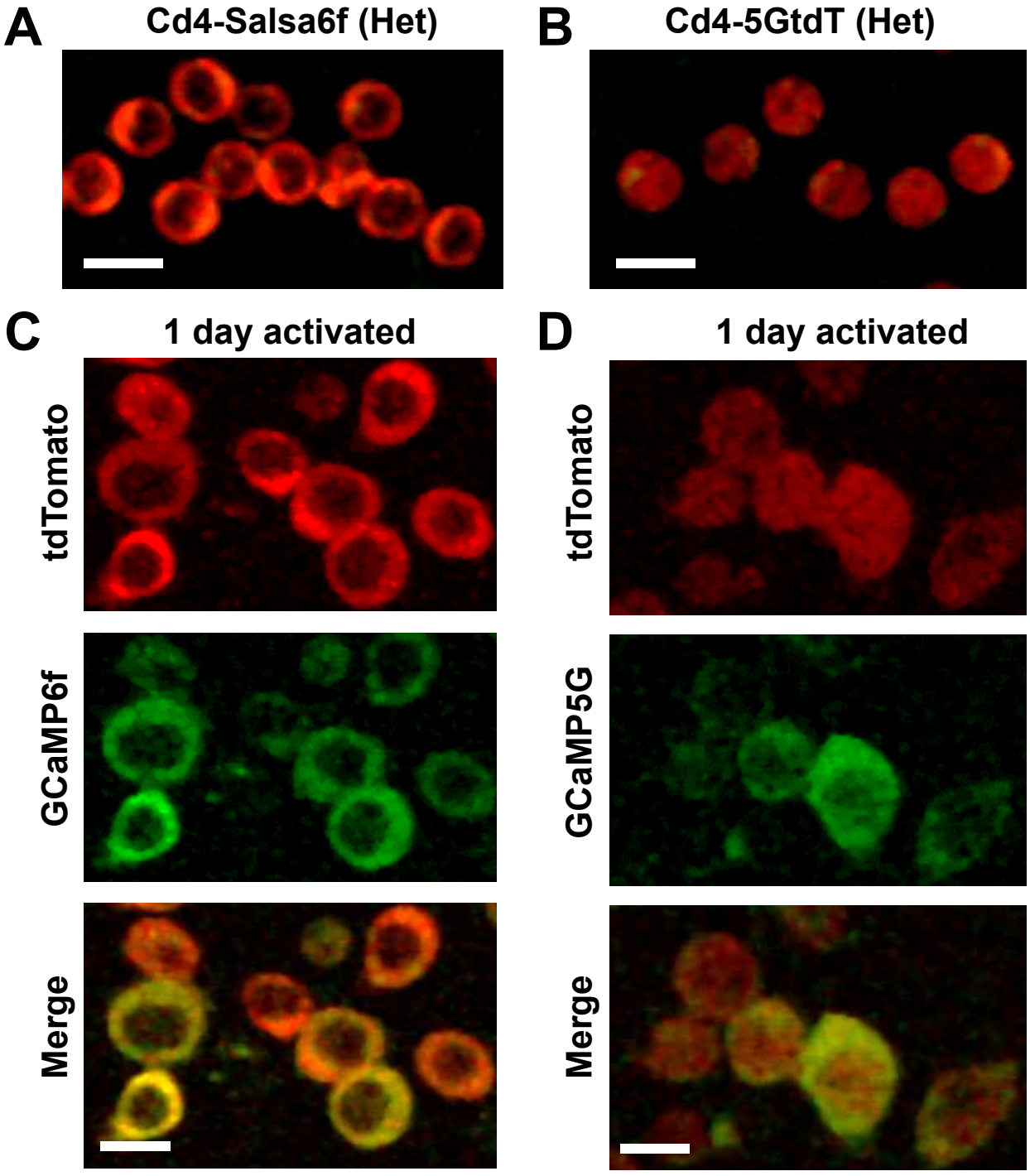

Figure 7

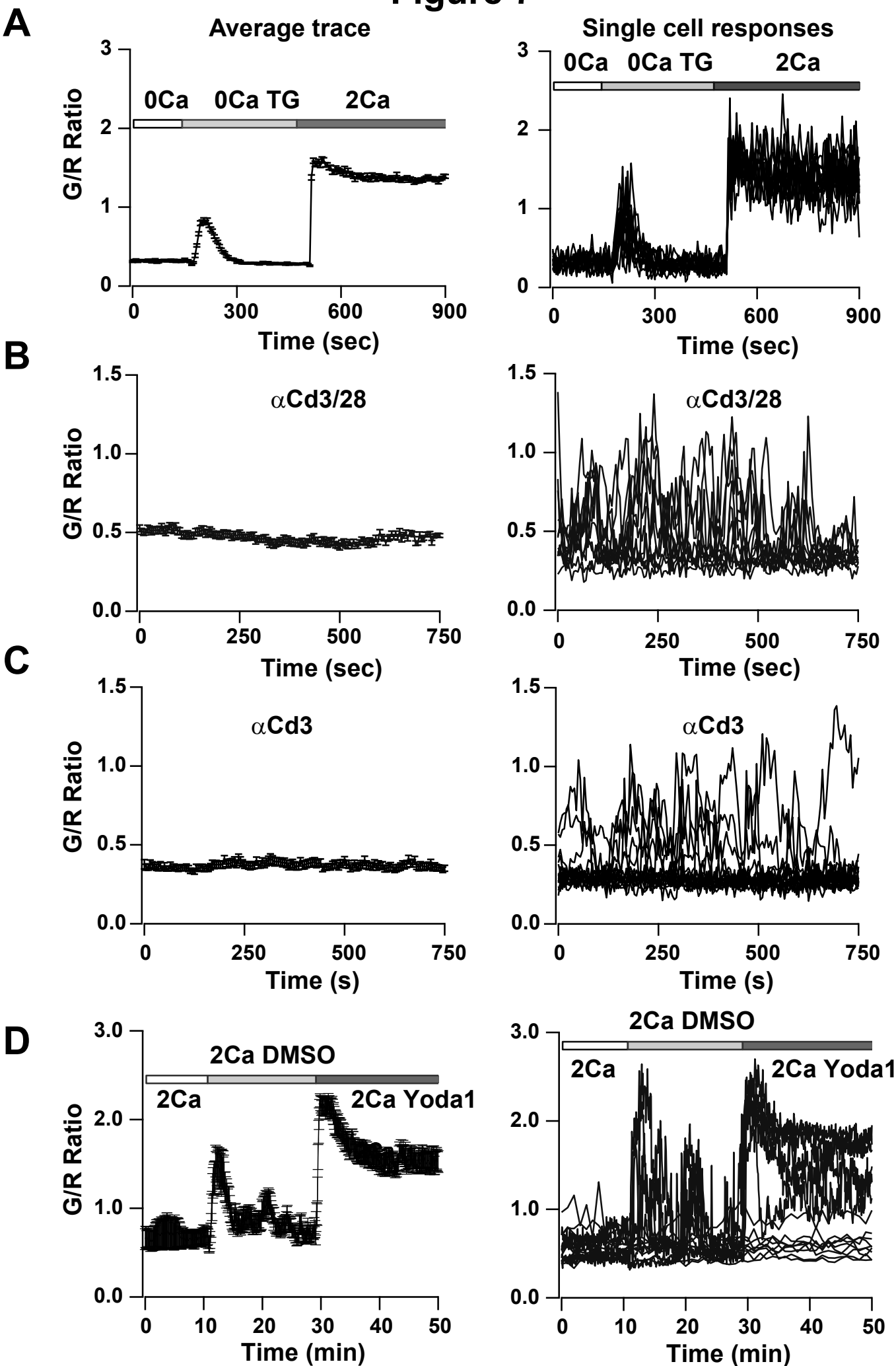
A
Average trace
Single cell responses
0Ca
0Ca TG
2Ca
G/R Ratio
Time (sec)
B
αCd3/28
C
αCd3
Time (s)
D
2Ca DMSO
2Ca Yoda1
Time (min)

Figure 7- Figure supplement 1

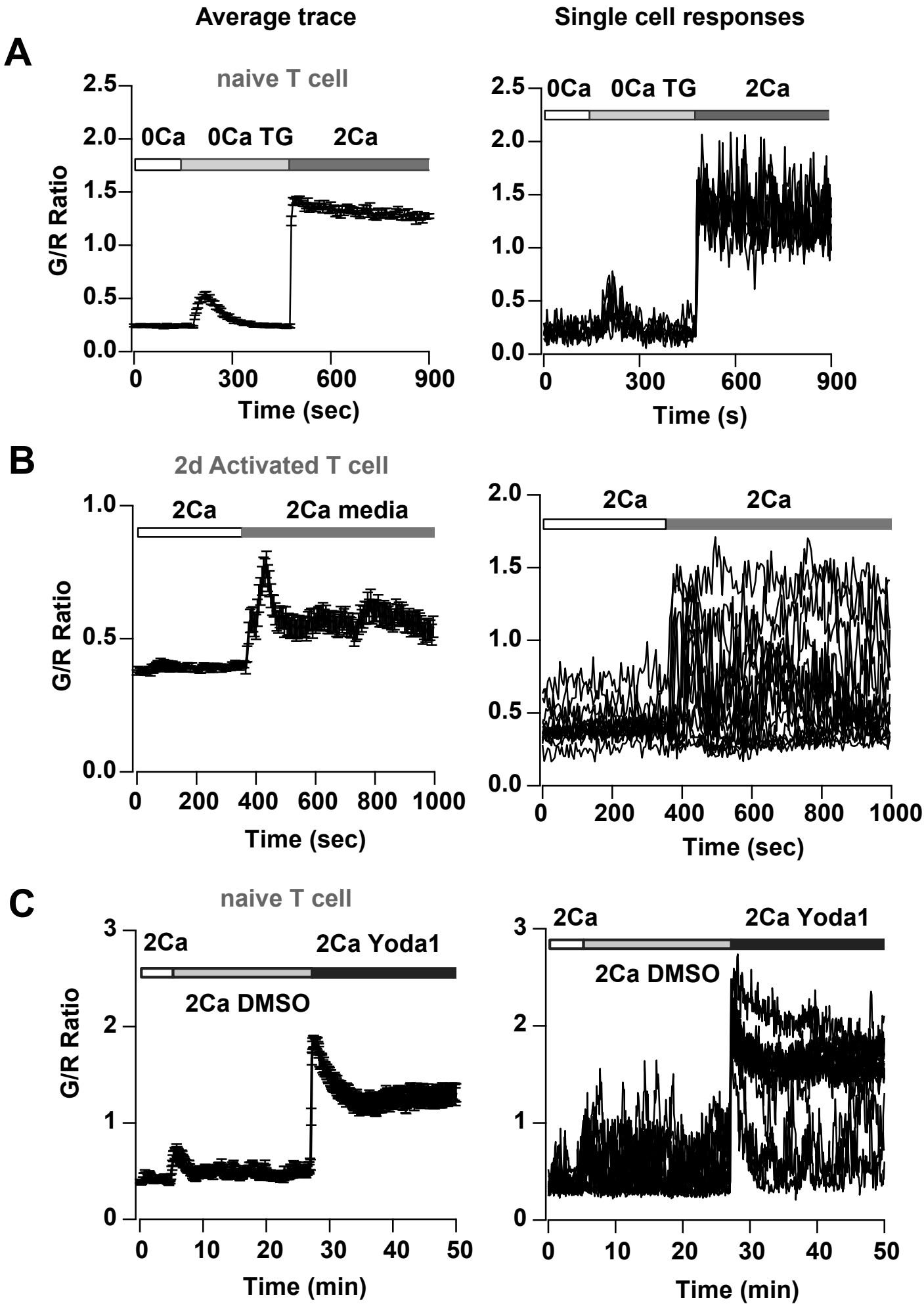

Figure 8

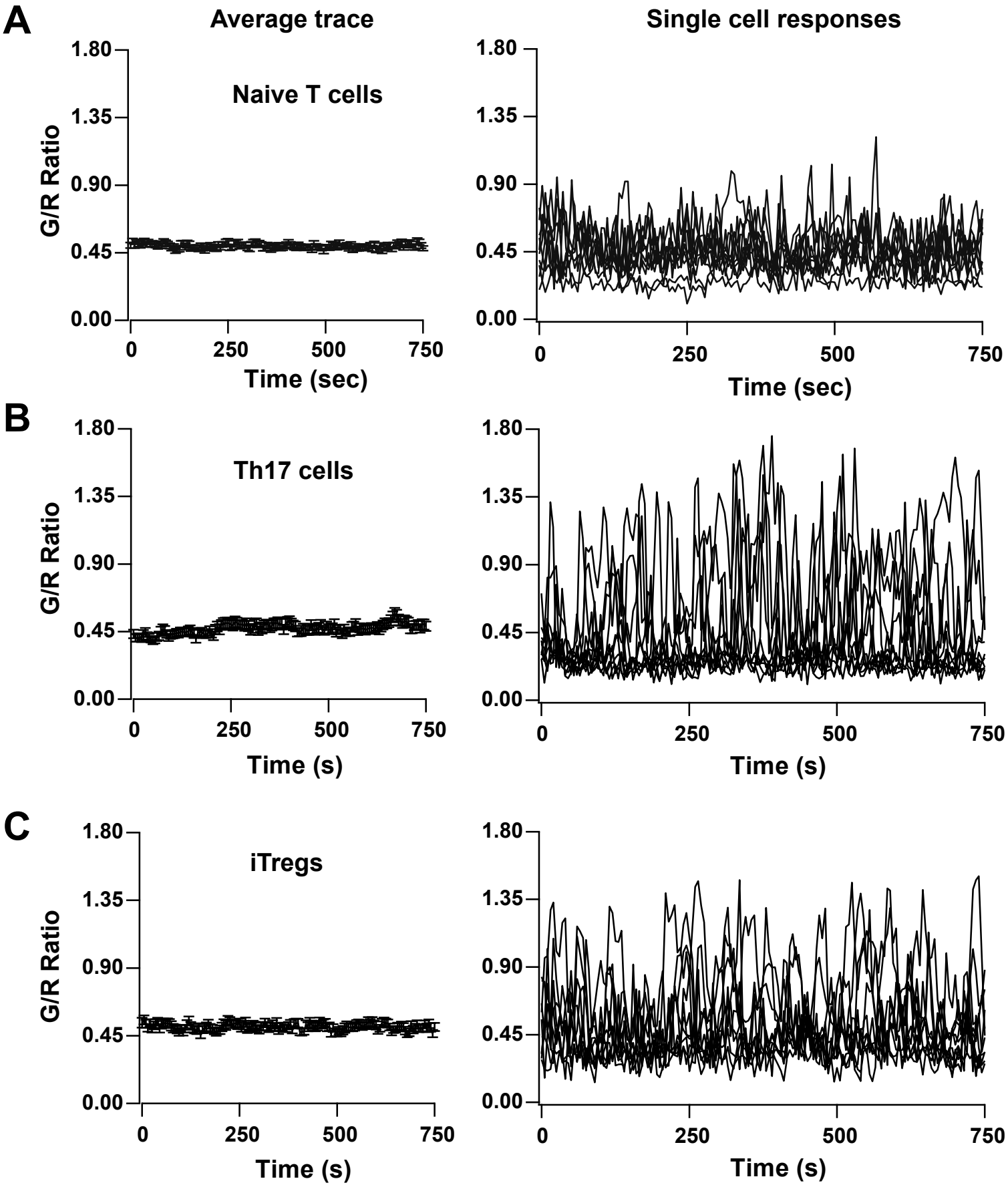
A
Average trace
Single cell responses
Naive T cells
G/R Ratio
1.80
1.35
0.90
0.45
0.00
0
250
500
750
Time (sec)
B
Th17 cells
Time (s)
C
iTregs

Figure 9

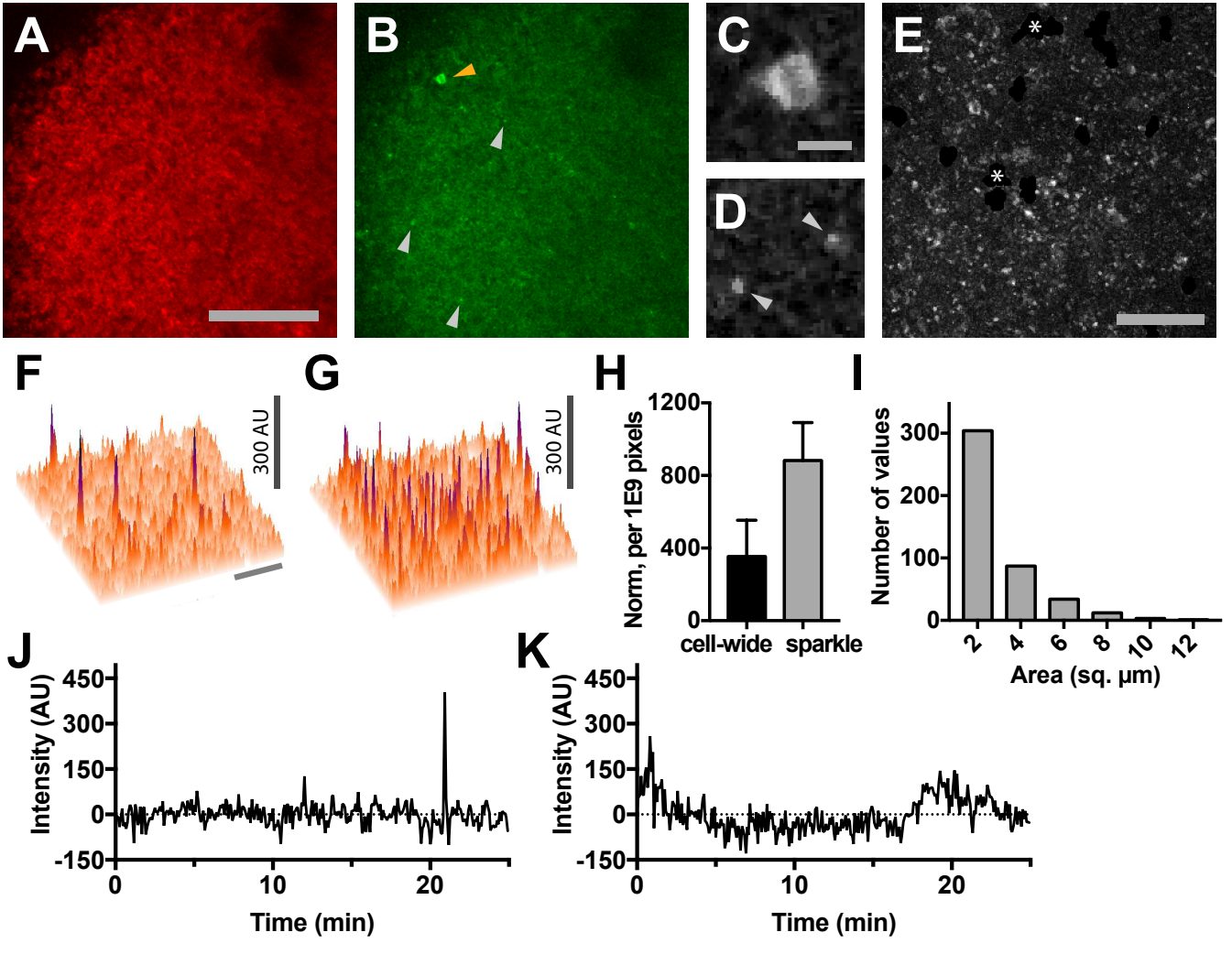
A
B
C
D
E
F
300 AU
G
300 AU
H
Norm, per 1E9 pixels
1200
800
400
0
cell-wide
sparkle
I
Number of values
300
200
100
0
2
4
6
8
10
12
Area (sq. µm)
J
Intensity (AU)
450
300
150
0
-150
0
10
20
Time (min)
K
Intensity (AU)
450
300
150
0
-150
0
10
20
Time (min)

Figure 9 - Figure supplement 1

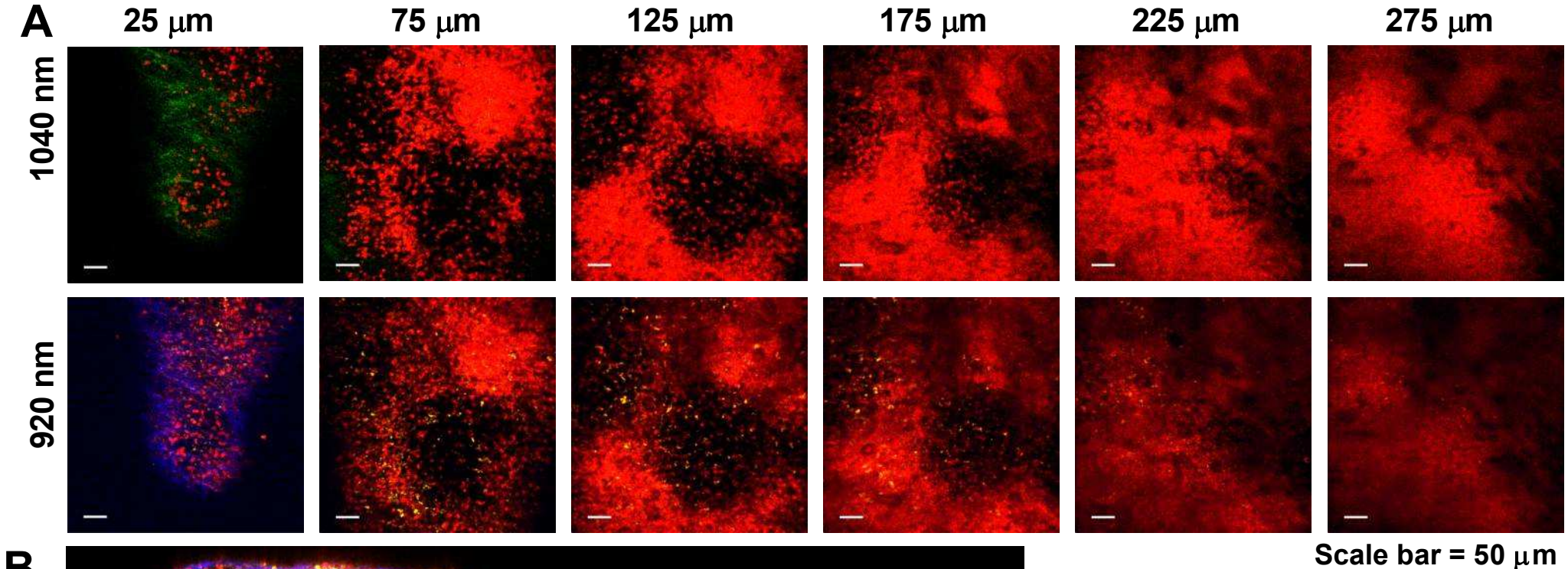

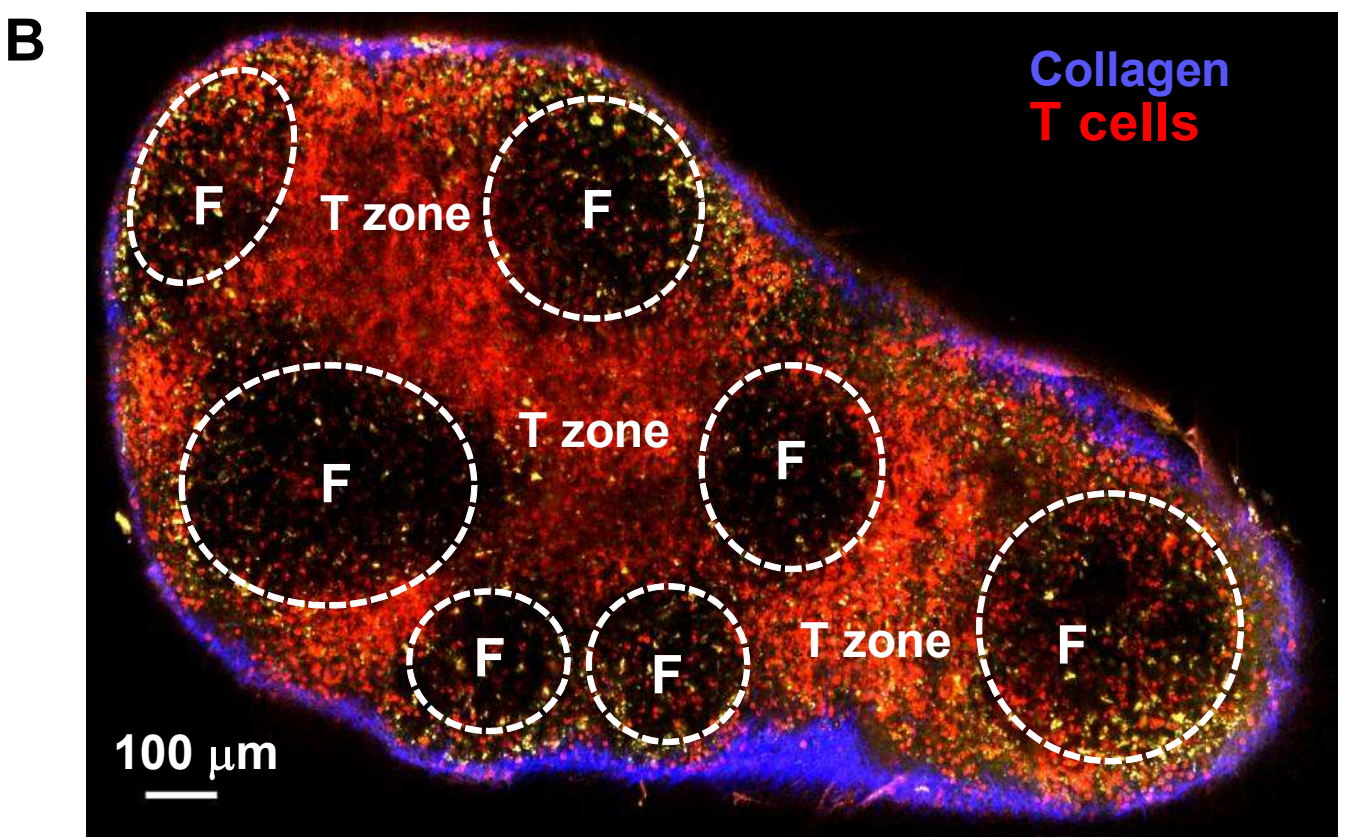

Figure 9- Figure Supplement 2

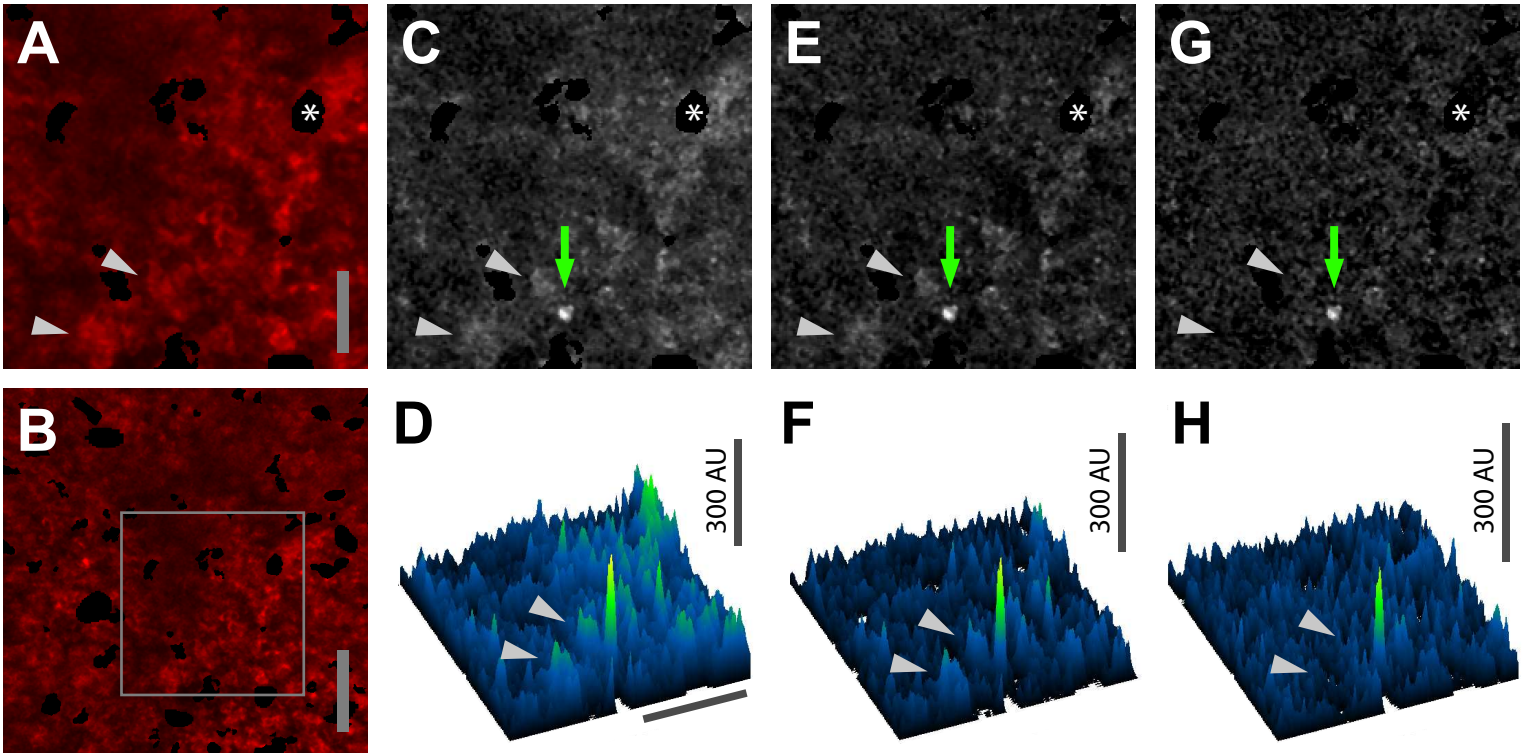

Figure 10

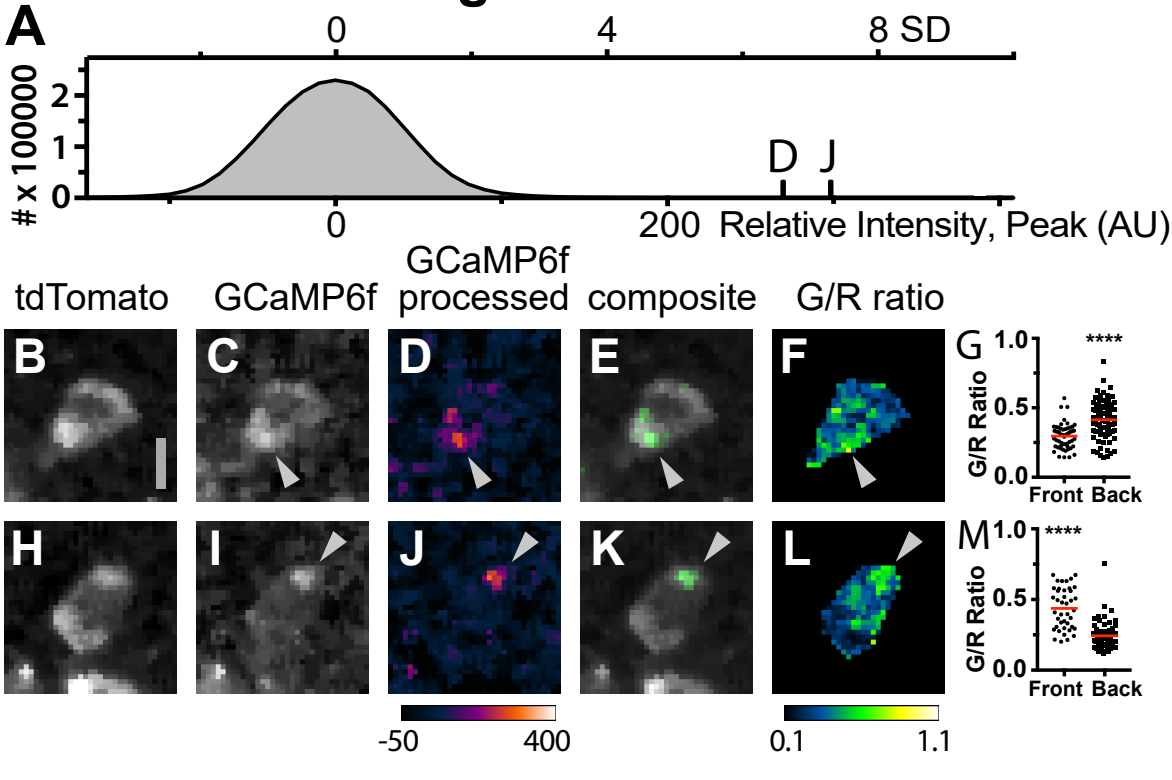
A
0
4
8 SD
x 100000
2
1
0
D
J
0
200
Relative Intensity, Peak (AU)
tdTomato
GCaMP6f
GCaMP6f processed
composite
G/R ratio
B
C
D
E
F
G
1.0
0.5
0.0
G/R Ratio
****
Front
Back
H
I
J
K
L
M
1.0
0.5
0.0
G/R Ratio
****
Front
Back
-50
400
0.1
1.1